

## ***An inside look at a biofilm: Pseudomonas aeruginosa flagella bio-tracking***

***Eden Ozer<sup>1,†</sup>, Karin Yaniv<sup>3,†</sup>, Einat Chetrit<sup>4</sup>, Anastasya Boyarski<sup>5</sup>, Michael M. Meijler<sup>5,6</sup>, Ronen Berkovich<sup>2,4</sup>, Ariel Kushmaro<sup>2,3\*</sup>, Lital Alfonta<sup>1,2,5,\*</sup>***

† These authors contributed equally.

<sup>1</sup>Department of Life Sciences, Ben-Gurion University of the Negev, POBox 653, Beer-Sheva 8410501, Israel.

<sup>2</sup>Ilse Katz Institute for Nanoscale Science and Technology, Ben-Gurion University of the Negev, POBox 653, Beer-Sheva 8410501, Israel.

<sup>3</sup>Avram and Stella Goldstein-Goren Department of Biotechnology Engineering, Ben-Gurion University of the Negev, POBox 653, Beer-Sheva 8410501, Israel.

<sup>4</sup>Department of Chemical Engineering, Ben-Gurion University of the Negev, POBox 653, Beer-Sheva 8410501, Israel.

<sup>5</sup>Department of Chemistry, Ben-Gurion University of the Negev, POBox 653, Beer-Sheva 8410501, Israel.

<sup>6</sup>National Institute for Biotechnology in the Negev, Ben-Gurion University of the Negev, POBox 653, Beer-Sheva 8410501, Israel.

\* Corresponding authors e-mails: [arielkus@bgu.ac.il](mailto:arielkus@bgu.ac.il); [alfontal@bgu.ac.il](mailto:alfontal@bgu.ac.il)

## **Abstract**

The opportunistic pathogen, *Pseudomonas aeruginosa*, a flagellated bacterium, is one of the top model organisms for studying biofilm formation. In order to elucidate the role of the bacterial flagella in biofilm formation, we developed a new tool for flagella bio-tracking. We have site-specifically labeled the bacterial flagella by incorporating an unnatural amino acid into the flagella monomer via genetic code expansion. This enabled us to label and track the bacterial flagella during biofilm maturation. Direct, live imaging revealed for the first-time presence and synthesis of flagella throughout the biofilm lifecycle. To ascertain the possible role of the flagella in the strength of a biofilm we produced a “flagella knockout” strain and compared its biofilm to that of the wild type strain. Results showed a one order of magnitude stronger biofilm structure in the wild type in comparison to the flagella knockout strain. This suggests a newly discovered structural role for bacterial flagella in biofilm structure, possibly acting as a scaffold. Based on our findings we suggest a new model for biofilm maturation dynamic and underscore the importance of direct evidence from within the biofilm.

**Keywords:** *Pseudomonas aeruginosa*, Genetic code expansion, Flagella, Biofilm formation

1       **Main**

2           *Pseudomonas aeruginosa* (*P. aeruginosa*) is a well-studied opportunistic pathogen<sup>1</sup>.  
3 Despite the fact that quorum-sensing and biofilm formation have been studied for the past 40  
4 years, new information is constantly being reported<sup>2,3</sup>. Biofilms provide a more resistant form of  
5 existence for bacteria than their planktonic forms, proffering them with protection from possible  
6 stressors. They therefore, have been intensely studied for their complexity and the mechanisms  
7 involved in their life cycle<sup>4,5</sup>. Indeed, any new information emerging from these studies is  
8 crucial, allowing the development of new and diverse strategies to resist infections.

9           The biofilm lifecycle is composed of several commonly reported steps<sup>1,6-8</sup>. Initially,  
10 planktonic bacteria propel themselves to a proximal surface, followed by an irreversible  
11 attachment to the surface. Once attachment is established, exo-polymeric substances are secreted  
12 from within the cells to generate a matrix of a supporting microenvironment for the dividing  
13 cells and to initiate formation of micro-colonies. Next, mushroom-like structures start to emerge.  
14 Finally, the cells secrete enzymes to digest the exo-polymeric substances at the top of the grown  
15 mushroom-like structures where the newly flagellated cells are released in a planktonic form to  
16 attach to new exposed surfaces.

17           The flagella, the bacterial rotor with its unique structure, is therefore an inseparable part  
18 of biofilm research<sup>9</sup>. Several reports have expressed a consensus regarding the importance of  
19 flagella in biofilm formation, specifically in its initiation<sup>10</sup>. However, despite a consensus among  
20 researchers that flagella are not present during biofilm maturation but only in the dispersion  
21 stage, reports regarding this are still somewhat constradicting<sup>10-16</sup>. Therefore, it is necessary to  
22 assess the presence and possible role of flagella in biofilms. Direct imaging of these organelles  
23 inside a developing biofilm may thus shed a better light on their role in biofilm formation and

24 maintenance as well as provide an improved understanding of what occurs during the biofilm  
25 lifecycle.

26 To date, live-cell imaging can be obtained through different approaches, however genetic  
27 code expansion, the reassignment of codons and incorporation of an unnatural amino acid (Uaa)  
28 into proteins<sup>17</sup>, displays advantages over other methodologies, and is gaining increasing exposure  
29 and momentum<sup>18-21</sup>. Genetic code expansion systems are being constantly improved, expanded  
30 and adapted to a growing number of organisms<sup>22-25</sup>. This technique aids in improving imaging.  
31 For example, the incorporation of a Uaa may alleviate the need for large and bulky labeling  
32 agents, such as fluorescent proteins or antibodies. Moreover, a protein with a site-specifically  
33 incorporated Uaa can be labeled using bio-orthogonal chemistry and serve as a specific reporter  
34 inside cells. Incorporating Uaa into *P. aeruginosa* flagellum enables live-cell imaging of flagella  
35 inside the complex environment of a biofilm. Herein, we present a robust and orthogonal genetic  
36 code expansion system in *P. aeruginosa* designed for flagella labeling for *in-vivo* flagella bio-  
37 tracking in a live and growing biofilm that revealed novel information regarding the biofilm  
38 lifecycle.

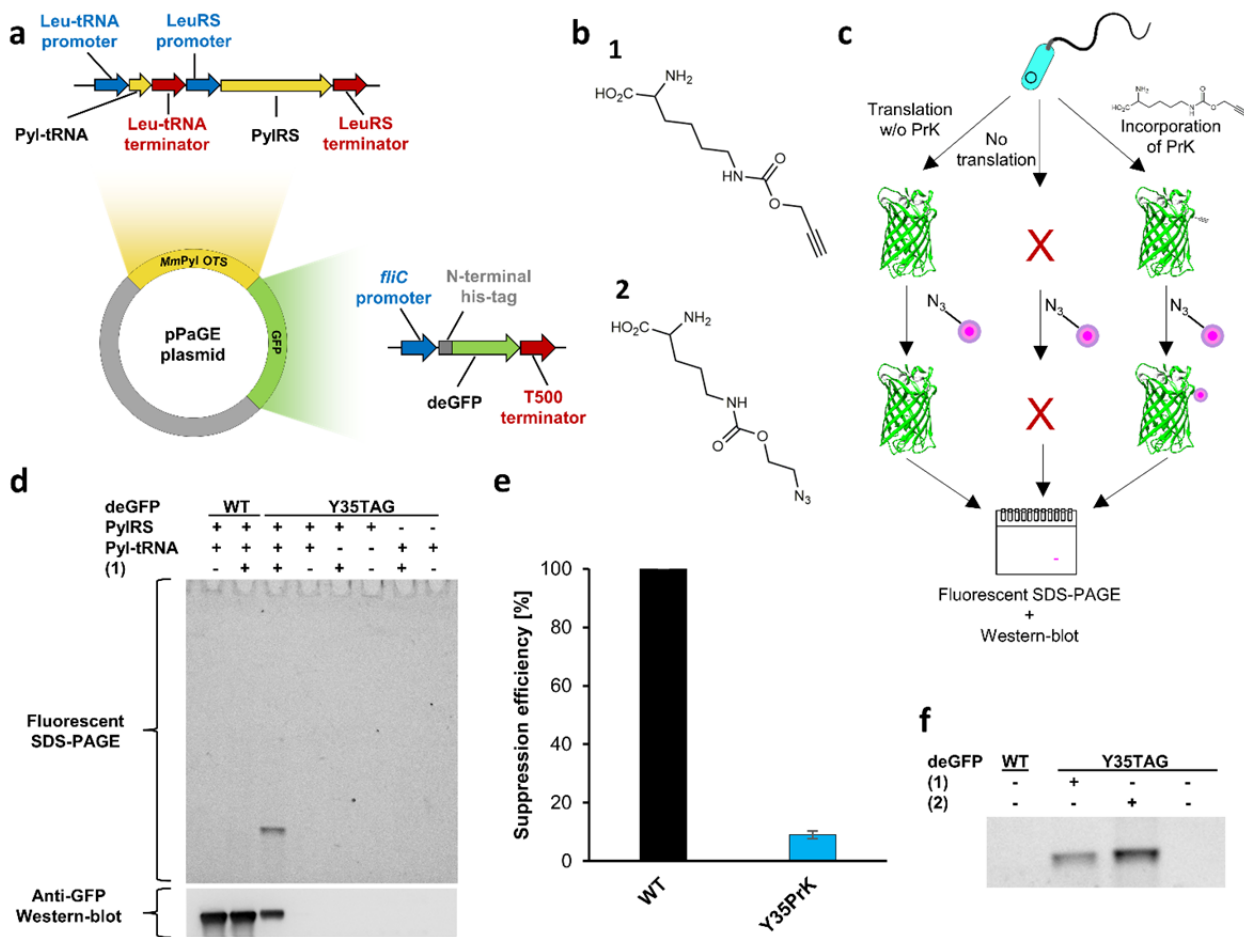
## 39 **Results**

40 **Genetic code expansion of *P. aeruginosa*.** For a Uaa incorporation into *P. aeruginosa*  
41 proteins, a new plasmid was constructed (Fig. 1a). The plasmid harbors an orthogonal translation  
42 system (OTS), as well as a reporter gene for system validation. An OTS, composed of a tRNA  
43 and tRNA-synthetase pair, could be considered orthogonal if it does not interact with native  
44 translational components<sup>26</sup>. *Methanosarcina mazei* pyrrolysyl orthogonal translation system<sup>27</sup>  
45 (*MmPyl* OTS) has been previously found to be orthogonal in several organisms, including gram-

46 negative bacteria, and was therefore our choice. Combined with *MmPyl* OTS, a GFP reporter  
47 gene encoded for Uaa incorporation.

48 The *P. aeruginosa* genetic code expansion plasmid (pPaGE) was assembled using *P.*  
49 *aeruginosa* endogenous promoters and terminators. Our rationale was that the bacterium will  
50 benefit from an attempt to maintain physiologically relevant expression levels of an exogenous  
51 OTS. We thus identified the most abundant codon in *P. aeruginosa* PAO1 genome<sup>28</sup>, which was  
52 found to be the CUG codon encoding for leucine (Leu). The native promoters and terminators of  
53 Leu-tRNA and Leucil-tRNA-synthetase were assigned as the upstream and downstream regions  
54 of Pyl-tRNA and Pyl-tRNA-synthetase respectively. Planning a future expression of flagella  
55 protein, the *fliC* endogenous promoter for flagellin expression, was chosen to serve as a promoter  
56 for the GFP reporter in the pPaGE plasmid. Toxicity tests for the Uaas: propargyl-L-lysine (PrK  
57 **(1)**) and azido-carboxy-lysine (AzCK **(2)**) (Fig. 1b.1 and Fig. 1b.2, respectively) were performed  
58 and have shown normal growth rates (Fig. S1).

59



60

61 **Figure 1| Genetic code expansion system of *P. aeruginosa* using GFP.** (a) Plasmid map of pPaGE. (b) Uaas  
 62 used in this study, PrK (1) and AzCK (2). (c) Schematic representation of possible translation outcomes for mid-  
 63 gene TAG mutants. (d) Lysed samples following a click reaction to an azide-containing fluorophore analyzed  
 64 through fluorescent SDS-PAGE and anti-GFP Western-blot analyses. (e) Suppression efficiency of GFP Y35PrK  
 65 mutant. (f) Lysed samples following a click reaction to either an azide or an alkyne containing fluorophore analyzed  
 66 through fluorescent SDS-PAGE.

67

68 We reassigned the TAG stop-codon for site-specific incorporation of Uaas and  
 69 introduced a TAG mutation to the GFP reporter gene at its 35<sup>th</sup> site. *MmPyl* OTS orthogonality in  
 70 *P. aeruginosa* was tested next. Several protein elongation scenarios for a premature TAG  
 71 introduction to GFP were tested, as well as the possibility of non-specific incorporation of a Uaa  
 72 into the host organism proteome (Fig. 1c, Fig. 1d). For that purpose, pPaGE variants containing  
 73 partial OTSs were generated by the removal of Pyl-tRNA or Pyl-tRNA-synthetase (PylIRS). Cells  
 74 were grown, lysed and analyzed using fluorescent chemical conjugation and anti-GFP Western-

75 blot analyses (Fig. 1d). In order to incorporate **(1)** into GFP, a click reaction using Cu(I)-  
76 catalyzed azide-alkyne cycloaddition (CuAAC)<sup>29</sup> to an azide-bearing fluorophore was conducted.  
77 Since there are no endogenous alkynes in bacteria, this experiment was meant to reveal whether  
78 there exists any **(1)** that was misincorporated in response to the TAG stop-codon in the bacterial  
79 proteome. Another possibility that needed to be ruled out was if PylRS can aminoacylate  
80 endogenous tRNAs, where **(1)** would have been incorporated into random locations in the  
81 genome. Both scenarios, resulting in non-specific fluorescent labeling into endogenous proteins.  
82 On the other hand, if Pyl-tRNA is not orthogonal and is aminoacylated by the host organism's  
83 tRNA-synthetases by natural amino acids, full-length GFP may still be synthesized and observed  
84 in the Western-blot.

85         When examining all the protein expression options as seen in Figure 1d, we did not  
86 observe fluorescent labeling or GFP expression in the presence of the partial OTS variants. This  
87 directly proved *MmPyl* OTS's orthogonality for the first time. Following the establishment that  
88 our system is indeed orthogonal, we were then able to analyze proper Uaa incorporation into  
89 GFP. Wild type (WT) GFP expression was observed either in the presence or absence of **(1)** and  
90 could be seen only in the Western-blot analysis and not in the fluorescent gel. This indicated that  
91 there was no incorporation of **(1)** into WT GFP. When the whole OTS was present together with  
92 **(1)**, a fully elongated GFP was detected in the Western-blot analysis. In addition, a clear  
93 fluorescent labeling corresponding to GFP in size was visible. This not only indicated that the  
94 reporter gene was able to be synthesized but also verified the presence of **(1)** inside the protein.  
95 Indeed, when those cells were grown in the absence of **(1)**, no expression was observed,  
96 signifying that the expressed protein was not a result of a read-through event by any natural  
97 amino acid. Final validation was performed using electrospray mass spectrometry (ESI-MS)

98 (Fig. S2), where the deconvoluted mass corresponded to GFP molecular weight with the desired  
99 (1) at position 35 instead of a tyrosine in the WT protein. Thus, it was concluded that Uaa was  
100 successfully incorporated and encoded for, in a protein expressed in *P. aeruginosa*.

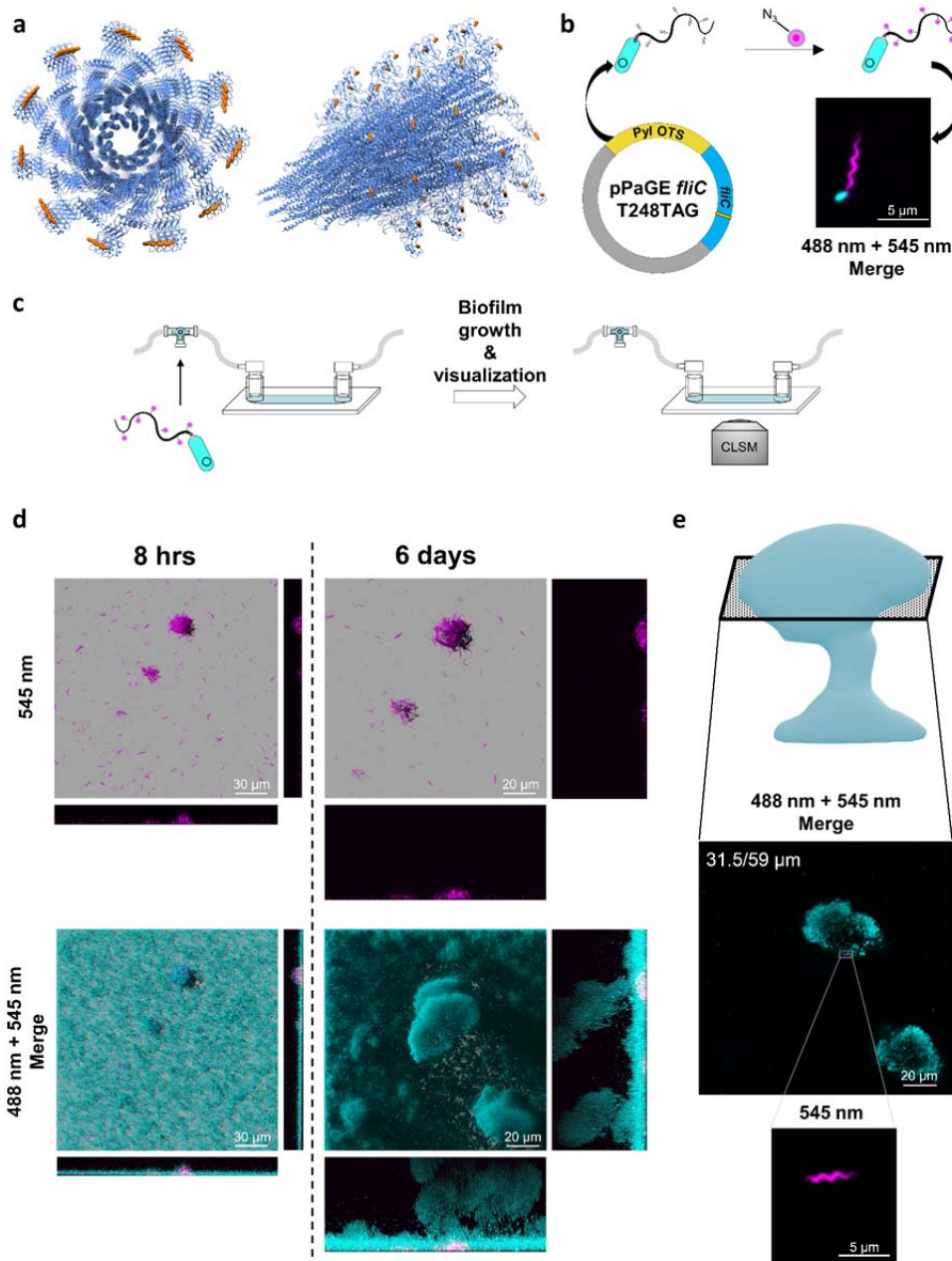
101       Suppression efficiency for Uaa incorporation into GFP was calculated as just under 10%  
102 (Fig. 1e). While offering information on the incorporation efficiency, it is important to note the  
103 context effects<sup>30</sup> at play in this methodology which may alter incorporation yields as well as  
104 suppression efficiency. For example, having the *fliC* promoter may impair incorporation into  
105 GFP but may be better for Uaa incorporation into a flagellin. In order to further establish the  
106 generated system following genetic code expansion with (1), (2) was also incorporated into GFP  
107 to test system's flexibility, moreover (2) has the ability to undergo a copper-free click  
108 chemistry<sup>29</sup> which makes it useful for future *in-vivo* applications. Here, (2) was also detected  
109 through copper-catalyzed click chemistry, this time to an alkyne-containing fluorophore, and  
110 resulted in positive incorporation (Fig. 1f). Thus, genetic code expansion was successfully  
111 achieved and the system's orthogonality was established in *P. aeruginosa*, using two different  
112 Uaas.

113       **Flagella “bio-tracking” in a biofilm.** Next, we incorporated a Uaa into the endogenous  
114 gene of flagella. The flagellum is a complex machinery composed of several genes and proteins  
115 that generates filaments extending up to 15  $\mu\text{m}$  in length<sup>31,32</sup>. Although assembled by a  
116 consortium of proteins, the flagellin protein encoded by the *fliC* gene is the repeating monomer  
117 subunit giving the flagellum its high aspect ratio. We decided to introduce modifications mainly  
118 in the D3 domain of flagellin, facing outwards in the cylindrical structure of flagellum, thus  
119 minimizing possible interference with filament assembly<sup>32</sup>. We modulated the *P. aeruginosa*  
120 flagellum that is composed of 41 subunits (based on PDB accession number 5wk5) with (1)



121 incorporated at flagellin's 248<sup>th</sup> position (Fig. 2a). This illustrates our ability to label the micro-  
122 structure by using a Uaa as a reactive bioorthogonal chemical handle, holding vast potential for  
123 bio-labeling and other applications.

124 We reasoned that replacing the native flagellin copy into the genome of *P. aeruginosa*  
125 with an incorporated Uaa may result in a short flagellum, leading to artifacts, as Uaa  
126 incorporation is a slower process than native amino acids incorporation<sup>33</sup>. For that reason, we  
127 chose an integrative approach: while encoding for a Uaa incorporation into the *fliC gene*  
128 harbored in the pPaGE plasmid, we still retained native flagellin in the genome for a hybrid  
129 assembly into a single unified flagellum. The integrated flagellum was thus predicted to have  
130 fewer chemical anchor points for bio-labeling. However, despite not having every monomer  
131 subunit carry a Uaa, this technique still allowed the micro-fiber to be labeled. Using the *fliC*  
132 promoter, the downstream sequence from the inserted *fliC gene* was also chosen as the native  
133 flagellin terminator, hence the sequence was completely identical to the native genomic sequence  
134 apart from the introduced premature TAG stop-codon mutation (Fig. 2b). The new plasmid was  
135 assembled and served for flagella genetic code expansion from that point onwards.



136

137 **Figure 2| Flagellin Uaa incorporation and inoculated flagella survival in a biofilm.** (a) Theoretical model of  
 138 *P. aeruginosa* flagella filament with incorporated (1) at the D3 domain (based on PDB accession number: 5WK5)  
 139 left: a top view; right: a side view, Uaa is an orange sphere. (b) Predicted system functionality and resulting  
 140 fluorescent imaging using confocal laser scanning microscopy (CLSM). Flagella with an incorporated Uaa were  
 141 labeled fluorescently (magenta) using PAO1 encoding genomic GFP reporter (gGFP) (cyan). Planktonic bacteria  
 142 were imaged with incorporated (1) in the flagellum. (c) Schematic representation of the flow-cell and experimental  
 143 setup for bio-tracking of flagella used for biofilm inoculation throughout biofilm maturation. Flagella with a Uaa  
 144 were fluorescently labeled and used as inoculation cells for continuous biofilm growth for up to 6 days. Biofilm  
 145 development and flagella were followed using CLSM. (d) Inoculated bacteria in a biofilm, pre-labeled prior to  
 146 inoculation, monitored inside biofilm's 3D structure development using CLSM. (e) Pre-labeled flagella located in a  
 147 mature biofilm at mid-height after 6 days of growth. Full scale and resolution images are available in the  
 148 supplementary information (SI) file Figs. S6-S11.

149 pPaGE *fliC* was transformed into *P. aeruginosa* and resulted in (1) incorporation into  
150 flagellin monomers (Fig. S3). It was also established that exogenous flagellin expression does  
151 not affect flagellum synthesis in each individual cell (Fig. S4). Next, the system was used for  
152 live-cell imaging using a click reaction. pPaGE *fliC* was inserted into *P. aeruginosa* PAO1 gGFP  
153 strain, carrying a genomic GFP reporter gene for the convenience of whole-cell detection. Using  
154 a confocal laser scanning microscope (CLSM), successfully labeled flagella were observed  
155 including its unique wave-like morphology features indicating a repetitive occurrence of the  
156 incorporated label (Fig. 2b, magenta). No signal was observed when expression was attempted in  
157 the absence of (1) (Fig. S5). Despite the fact that not every monomer was labeled, the generated  
158 filament was successfully visualized, and the unique wave-like feature of flagella was recorded.

159 With this new labeling tool, it was now possible to “bio-track” flagella inside a biofilm.  
160 This technique enabled us to track the labeled inoculated flagella, attached to the cells that were  
161 used to initiate biofilm formation. Hence, the following experimental setup was pursued (Fig.  
162 2c): *P. aeruginosa* expressing genomic GFP, harboring the pPaGE *fliC* plasmid were grown in  
163 the presence of (1). Planktonic bacteria containing (1) were fluorescently labeled by a click  
164 reaction and inserted into a flow-cell. Labeled bacteria were grown for up to 6 days, while  
165 inoculated flagella were monitored inside the biofilm every few hours. Labeled flagella, with  
166 their distinct morphology, were clearly observed after initial surface attachment and growth in  
167 the flow-cell either as singles or as clusters of different sizes (Fig. 2d). The emergence of flagella  
168 clusters was a notable observation that was not reported before.

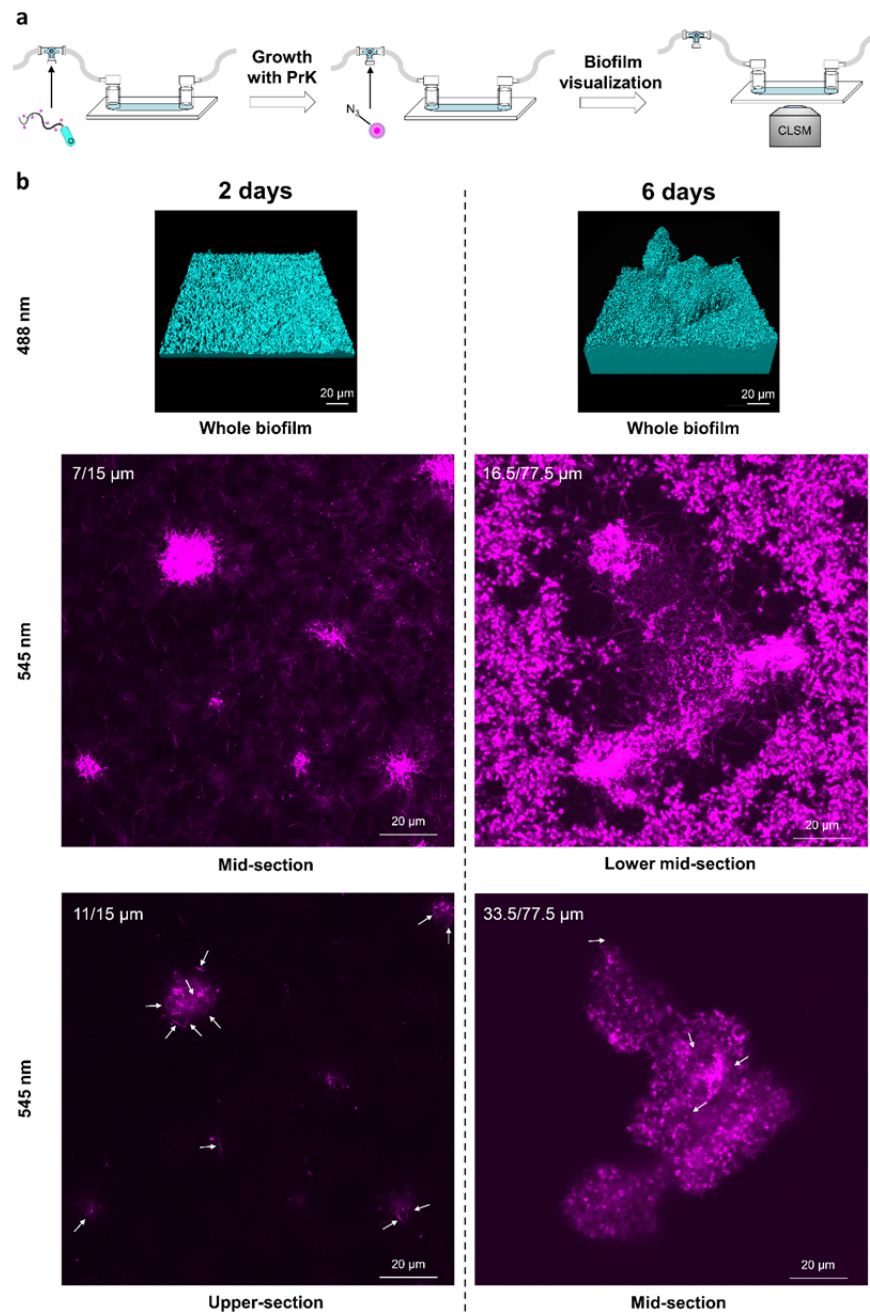
169 Flagella bio-tracking for a time period of up to 6 days of biofilm growth, enabled us to  
170 provide evidence regarding possible changes in the state of the flagella in a biofilm with time.  
171 For example, we could determine whether inoculated flagella are maintained or degraded within

172 the biofilm. We could demonstrate in a direct manner that despite continued biofilm growth to  
173 heights of above 59  $\mu\text{m}$  in total, the majority of flagella remained in approximately at the bottom  
174 of the biofilm in the first 13  $\mu\text{m}$  of the biofilm (Fig. 2d). While most flagella seemed to remain at  
175 the bottom of the biofilm, rarely we observed inoculated flagella in higher sections of a grown  
176 biofilm, found at around 31.5  $\mu\text{m}$  (Fig. 2e). That means that not only inoculated labeled flagella  
177 are still present and are not metabolized within the time frame of the experiment but also that  
178 occasionally, they might reach higher regions in the biofilm through an unknown mechanism.  
179 The notion of flagella movement inside the biofilm has been previously speculated in the  
180 literature<sup>13,14</sup>, however this is the first direct evidence for its occurrence. Indeed, the images  
181 presented here (Fig. 2e) serve as the first direct evidence to this hypothesis. It is important to  
182 note that due to imaging limitations, it is hard to determine if the observed flagella are still  
183 attached to a cell or not. However, individual flagella that are observed in the biofilm's mid-  
184 height were most likely positioned there due to a response to bacterial signaling. Hence, this has  
185 led us to believe that most of the observed flagella are indeed attached to bacterial cells.

186 **Flagella synthesis in a biofilm.** After locating the labeled inoculated flagella in the biofilm,  
187 we wanted to ascertain whether we could track newly synthesized flagella in the biofilm and if  
188 so, where are they located in the biofilm. The biofilm lifecycle is divided into several steps  
189 where planktonic cells transform and grow together into mushroom-like structures. Interestingly,  
190 throughout the biofilm's growth, flagella synthesis is halted and is only re-initiated during the  
191 final step of dispersion from the mature biofilm<sup>5,7,8,34-36</sup>. To date, the most accepted concept of  
192 flagella synthesis in a biofilm is that it occurs in a compartment located at the upper section of  
193 the mushroom-like structure in a grown biofilm. Therefore, using our system, we set out to label  
194 the compartments at the top of the mushroom-like structures in order to directly visualize flagella

195 inside them for the first time. Pre-labeled cells were used for flow-cell inoculation as before, but  
196 this time the media supply for the flow-cell contained (1) for continued Uaa incorporation inside  
197 the growing biofilm for 2,4 or 6 days. Following growth, the biofilm was re-labeled using the  
198 same fluorophore (Fig. 3a).

199



200

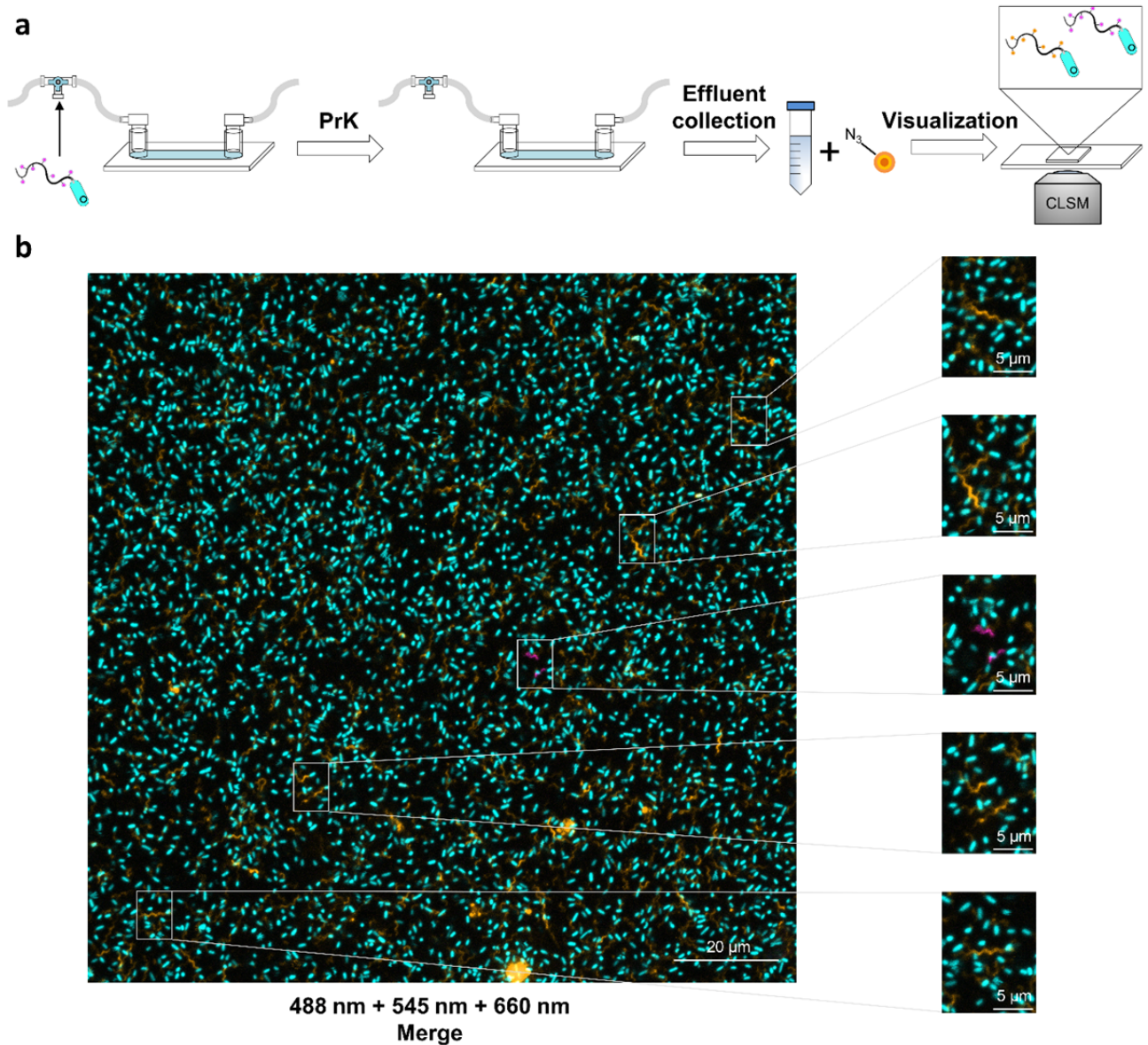
201 **Figure 3| Flagella synthesis during biofilm maturation.** (a) Schematic representation of the experimental  
202 setup identifying flagella synthesis within the biofilm. Flagella with incorporated Uaa were fluorescently labeled and  
203 used as inoculation for continuous biofilm growth in the presence of Uaa for up to 6 days. Flagella were  
204 fluorescently labeled inside the biofilm at different biofilm's growth time points of 2 and 6 days and visualized  
205 using CLSM. (b) CLSM imaging from within the biofilm at different growth stages. For each time point during  
206 biofilm maturation, biofilm was imaged, and flagella were documented at different heights of the biofilm. Bacteria  
207 labeled in cyan and flagella in magenta. Enlarged images, as well as four-day old biofilm images are available in  
208 Figs. S12-S26.

209 Large quantities of fluorophore were trapped inside the viscous exo-polymeric matrix of the  
210 biofilm<sup>6</sup> and appeared as a bulk cloud-like signal. Flagella did not appear at the top of the mature  
211 biofilm, while many flagella were observed at the lower and middle sections of the biofilm  
212 throughout its growth (Fig. 3b, images of 4 days old biofilm and Figs. S17-S21). In the two-day  
213 old biofilm, flagella were located throughout the entire biofilm up to the height of 15  $\mu\text{m}$  on  
214 average. A four-day old biofilm also had flagella at the base of the biofilm as well at the height  
215 of approximately 22  $\mu\text{m}$  out of 30.5  $\mu\text{m}$  in total. Finally, a mature six-day old biofilm had  
216 abundant and noticeable flagella at mid-height (33.5  $\mu\text{m}$ ) of the 77.5  $\mu\text{m}$  maximal height. These  
217 results not only confirmed our prediction of being able to detect flagella in the biofilm  
218 throughout its unique shape, but also contradicted the accepted consensus that flagella are  
219 located only at the top of mushroom-like structures in a mature biofilm.

220 Consistently seeing numerous flagella inside the biofilm throughout its whole lifecycle  
221 was unexpected. This is because according to the literature<sup>5,7,8,34-36</sup>, it appears that there is no  
222 flagella synthesis during biofilm growth. This notion was based mainly on indirect bulk-  
223 population analysis of DNA/RNA microarrays, total biomass calculations and proteomic  
224 analysis<sup>15,37-39</sup>. This discrepancy provides important evidence for the importance of direct  
225 flagella visualization from within the biofilm, at an appropriate spatio-temporal resolution. When  
226 new flagella were observed from the biofilm's base up to approximately mid-height, we could  
227 only assume that previously indirect analysis had an averaging effect on the population. Another  
228 accepted aspect was that flagella exist at the top of micro-colonies in young biofilms, to allow

229 flagella mediated movement in between micro-colonies<sup>13,14</sup>. A compartment containing flagella  
230 at the top of a mushroom-like structure in a grown biofilm or any flagella in higher regions were  
231 not observed even though they were easily detectable everywhere else in the biofilm.

232 Cells may detach from the mature biofilm by several ways; through erosion, bulk  
233 detachment or by planktonic release<sup>8</sup>. In order to ascertain the possible changes occurring in  
234 detaching cells, the Flow-cells' effluent was collected prior to whole biofilm labeling and was  
235 labeled using a second fluorophore (with different excitation and emission wavelengths) to  
236 distinguish between inoculated flagella and newly synthesized flagella (Fig. 4a). We collected  
237 the biomass into chilled tubes immediately upon their exit from the flow-cells. Thus, we could  
238 assume that any flagellum that was observed was synthesized inside the biofilm. Looking at the  
239 double-labeled effluent of a young biofilm, new flagella were clear and abundant. This meant  
240 that cells are frequently flagellated before leaving the biofilm (Fig. 4b). While correlating well  
241 with known dispersion mechanisms from a mature biofilm, we expected to observe flagellated  
242 cells leaving only the mature biofilm and were surprised by the continued flow of flagellated  
243 cells in the effluent of our flow-cell set-up. (Fig. 4b, Figs. S27-S38).



244

245 **Figure 4| Dispersed flagellated cells.** (a) Schematic representation of the experimental setup identifying  
246 dispersed cells from within the biofilm carrying synthesized flagella from before their release. Flagella with  
247 incorporated Uaa were fluorescently labeled and used as inoculation for continuous biofilm growth in the presence  
248 of Uaa for up to 6 days. Effluent was collected at different time points, labeled with a second, different fluorescent  
249 dye and visualized using CLSM. (b) CLSM imaging of dispersed flagellated cells from a two-day old biofilm.  
250 Bacteria labeled in cyan, inoculated flagella in magenta and new flagella in orange. Enlarged images, as well as  
251 dispersion images for 4-/6-day old biofilms, are available as Figs. S27-S38.

252

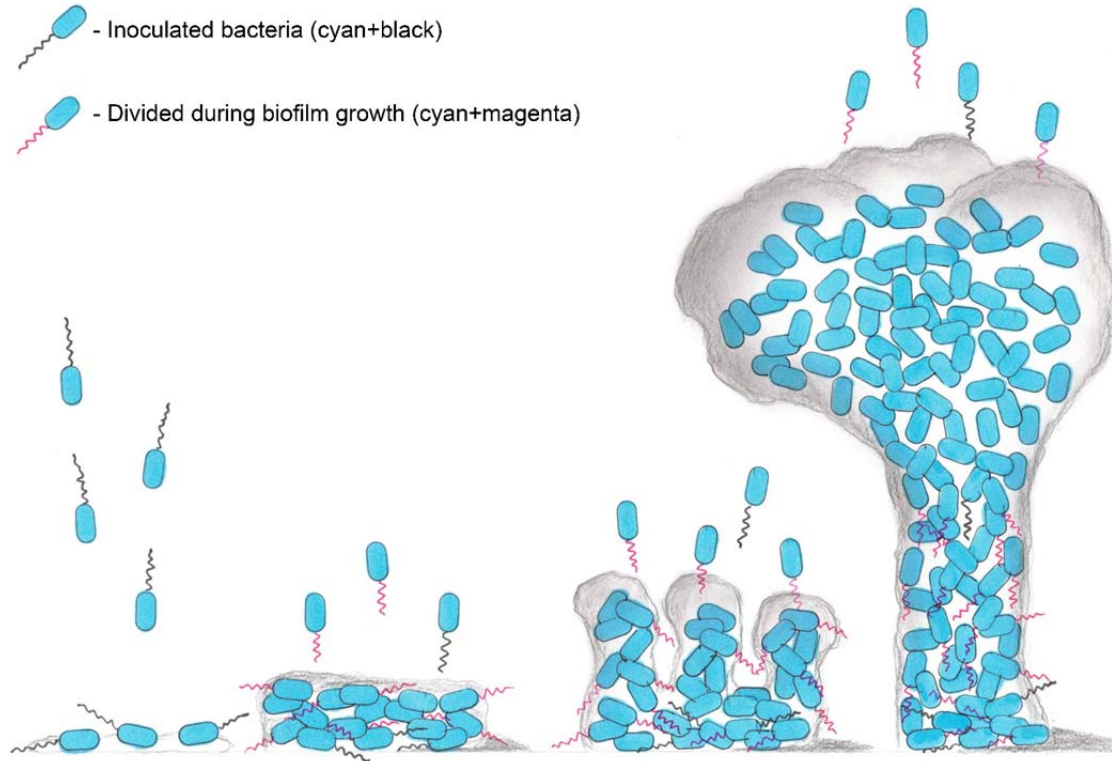
253 Examining many flagellated cells dispersed from the biofilm, we also detected very rare  
254 cases of labeled inoculated flagella (Fig. 4b). Although these observations were rare, indicating  
255 that this may be a statistical error when analyzed quantitatively, the image was clear and



256 reproducible. As mentioned previously, it is difficult to detect if the flagella that were observed  
257 in the biofilm were connected to cells or not. Despite this, we showed that labeled inoculated  
258 flagella were still attached to cells. This served as further support of our initial hypothesis,  
259 suggesting most of the observed flagella were indeed still connected to a cell and that they  
260 displayed some level of movement inside the biofilm.

261         Discovering continued flagellated dispersion is novel information regarding the biofilm  
262 lifecycle model and reflects the observation that the biofilm is filled with flagella as was  
263 discovered in this study. From a clinical aspect, mature biofilms are prone to planktonic  
264 dispersion at times, causing exacerbations in chronic infections and afflicting new environment  
265 within the host<sup>40</sup>. Usually, these exacerbations are in need of antibiotics treatment but are only  
266 taken under consideration in case of a mature biofilm. Hence, continuous planktonic cells release  
267 could affect the clinical view of possible treatments for chronic “biofilm infected” patients. All  
268 the information gathered in this work, enabled us to portray an updated and more accurate model  
269 for the biofilm lifecycle (Fig. 5).

270

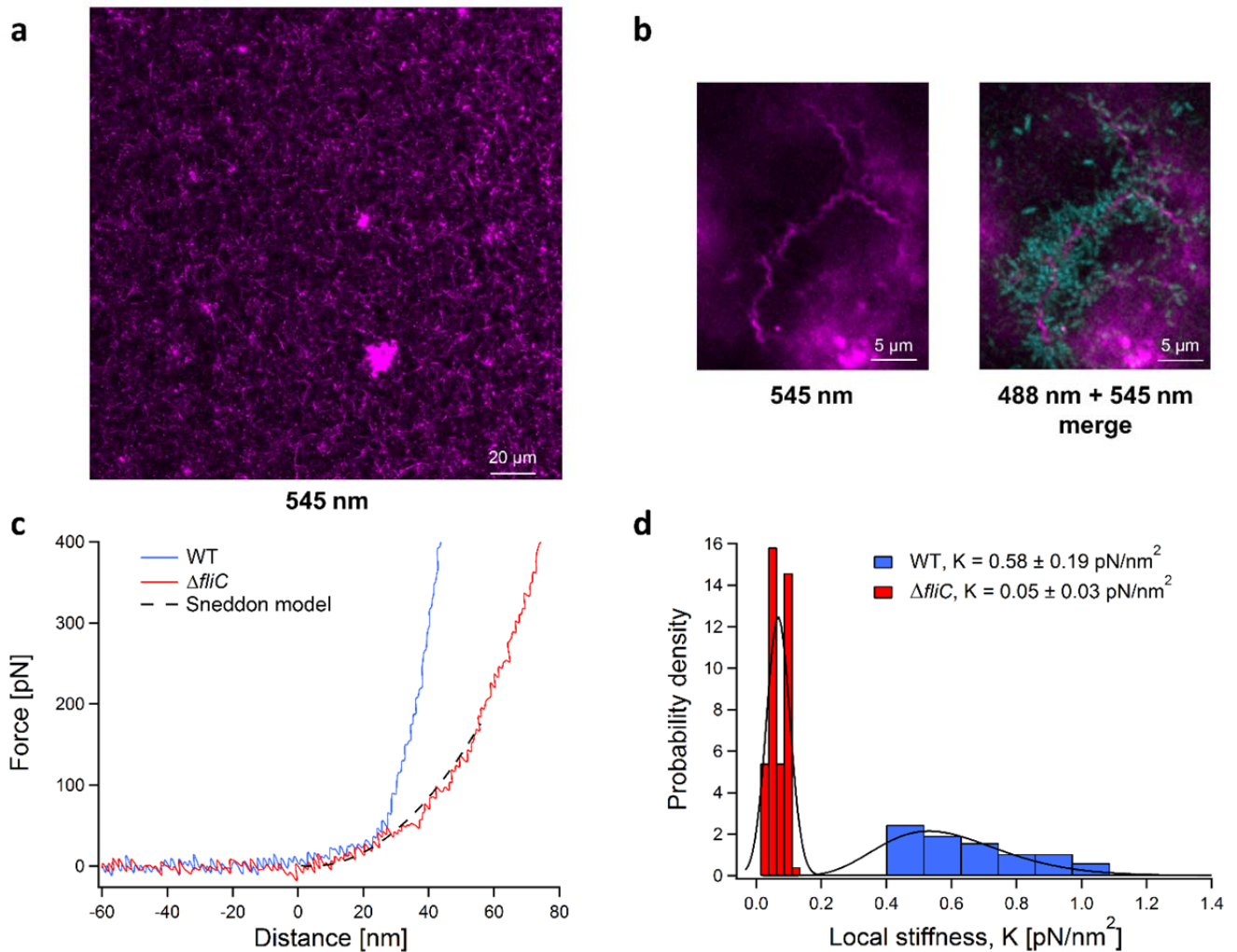


271

272 **Figure 5| Updated biofilm lifecycle model based on the presented discoveries.**

273 **Flagella's structural importance in a biofilm.** Learning that flagella are continuously being  
274 synthesized within a growing biofilm, we asked ourselves whether they might play a possible  
275 role in a biofilm mechanical structure. Considering that flagella synthesis is energetically costly<sup>41</sup>  
276 and that cells within the biofilm are mainly non-motile, there must be a reasonable explanation as  
277 to why the flagella are formed in cells inside the biofilm. We observed a visible grid-like  
278 appearance of the flagella in the lower part of the biofilm (Fig. 6a). In addition, we observed  
279 several bacteria assembling on a single flagellum as shown in Figure 6b. These observations  
280 seemed of importance as the structure resembled a structural scaffold that supports a substantial  
281 architecture. The idea of the role of flagella as a mechanical support in a biofilm has been  
282 previously suggested in *E. coli* macrocolony biofilms but has yet to be demonstrated<sup>42</sup>. An  
283 additional observation to support this hypothesis is the observation of *Geobacter sulfurreducens*

284 electrochemical-chamber biofilm in their cytochromes spatial arrangement on the flagella<sup>12</sup>. To  
285 investigate such a possible role of flagella for physical support, we constructed a *P. aeruginosa*  
286 strain that allows us to examine this notion.  
287



288

289 **Figure 6| Flagella as physical support in a biofilm microenvironment.** (a) CLSM imaging of the lower  
290 section of a four-day old biofilm with numerous flagella in a grid-like structure. (b) CLSM imaging of bacterial  
291 assembly on flagella in a growing biofilm. Bacteria labeled in cyan and flagella in magenta. Enlarged images are  
292 available as Figs. S39-S40. (c) Nanindentation force-distance curves of the WT biofilm (blue) and a  $\Delta fliC$  biofilm  
293 (red). The  $\Delta fliC$  curve is fitted with the Sneddon model (dashed black line), from which K, the local stiffness  
294 modulus was estimated. (d) Local stiffness probability density distributions of WT biofilm (blue) and  $\Delta fliC$  biofilm  
295 (red). The distributions were fitted by relevant statistical models (black line), from which their means and standard  
296 deviations were calculated.

297 Using CRISPR Cas9 for genome editing, based on *Streptococcus pyogenes* Cas9 which was

298 adapted for *P. aeruginosa* genome editing<sup>43</sup>, we generated a sub-strain lacking the ability to

299 produce flagella. This was carried out by deleting the flagellin gene ( $\Delta fliC$ ) from the *P.*  
300 *aeruginosa* genome. Transmission electron microscope (TEM) imaging and the loss of its  
301 swarming abilities validated that the new strain does not express flagella (Fig. S41). We then  
302 attempted to identify differences between WT and  $\Delta fliC$  based biofilms. We hypothesized that  
303 mushroom-like structures will be affected by the absence of flagella. Despite this, we could not  
304 detect any distinct gross morphological differences between the two biofilms (Fig. S42).  
305 However, high-resolution scanning electron microscopy (HR-SEM) revealed noticeable visual  
306 difference between the two biofilms (Fig. S43). WT biofilm possessed fibers forming a web  
307 between the cells, while in the  $\Delta fliC$  biofilm cells were much more crowded and there were  
308 significantly less fibers. Since multiple string-like fibers were present in the biofilm and  
309 represented the complex environment surrounding the cells (sugars, proteins, DNA, etc.) it was  
310 not possible to use regular microscopic methods to determine morphologically which elements  
311 are flagella and which are not. Therefore, further comparison was performed using atomic force  
312 microscopy (AFM) on WT and  $\Delta fliC$  biofilms (Fig. S44). Though we did not find an indication  
313 in these images for the structural importance of the flagella to the biofilm, flagella were easily  
314 recognized within the WT biofilm. This serves as further validation of the consistent presence of  
315 flagella in the biofilm.

316 Hypothesizing that flagella contribute to the strength of the biofilm's structure, we  
317 decided to inspect the biofilm's mechanical strength and stiffness. A biofilm's mechanical  
318 strength is important to its survival. This characteristic is being actively studied in order to better  
319 understand the contribution of different elements to the exo-polymeric environment or to  
320 measure biofilm's resilience following different treatments<sup>44-46</sup>. For that purpose, we used AFM  
321 nanoindentation measurements on the two variants' mature biofilms. If the hypothesis is correct

322 and the flagella take part in the biofilms' structural strength, then a biofilm lacking flagella  
323 should be mechanically weaker. Figure 6c shows examples of WT and  $\Delta fliC$  (marked as blue and  
324 red, respectively) biofilm force-distance traces obtained from the nanoindentation measurements.  
325 Each indentation curve demonstrates specific elastic response. There is a clear difference in the  
326 elastic response curvatures for the two biofilms indicating lower local stiffness for the  $\Delta fliC$   
327 biofilm. Fitting the curves with the Sneddon model allowed the estimation of local elastic  
328 stiffness,  $K$ , as illustrated for the  $\Delta fliC$  biofilm (Fig. 6c black dashed line).

329 We analyzed 100 force-distance curves collected for each of the biofilms, enabling the  
330 estimation of local stiffness and verification that the biofilms did not undergo irreversible  
331 deformation. The local stiffness,  $K$ , was collated into probability density functions that  
332 interestingly displayed two spreading behaviors. While the stiffness of the  $\Delta fliC$  displayed a  
333 narrow normal distribution, the stiffness of the WT biofilm showed a wide heavy tail  
334 distribution. This means that the stiffness values of the WT biofilm spread over a wider range  
335 compared to those of the  $\Delta fliC$  biofilm, with stiffness values that can get considerably high. For  
336 this reason, the  $\Delta fliC$   $K$  probability distribution was fitted with a normal (Gaussian) distribution,  
337 and the WT  $K$  was fitted with Gamma distribution, in order to properly assess their collective  
338 values, i.e., means and standard deviations (Fig. 6d). Local stiffness value estimated for WT  
339 biofilm was one order of magnitude higher than  $\Delta fliC$  biofilm's local stiffness. This proved that  
340 the  $\Delta fliC$  biofilm is weaker in terms of physical strength ( $K_{WT} = 0.58 \pm 0.19$  pN/nm<sup>2</sup> vs.  $K_{\Delta fliC} =$   
341  $0.05 \pm 0.03$  pN/nm<sup>2</sup>). This result implied that, indeed, flagella take a crucial part in the biofilm  
342 mechanical strength, much like scaffolds in a construction.

343 In order to exemplify the importance of these findings we returned to the literature and  
344 found that in some cases, *P. aeruginosa* strains isolated from cystic fibrosis patients lack flagella

345 due to various mutations in flagella synthesis involved genes<sup>47</sup>. It was found that cystic fibrosis  
346 isolates occasionally develop differently, in order to evade the human immune system that  
347 mainly targets bacterial flagella. Recently, Harrison et. al.<sup>47</sup> revealed the connection between the  
348 loss of flagellum and overexpression of exopolysaccharides in biofilms created from cystic  
349 fibrosis isolates. The nanoindentation results presented here can elucidate further details on this  
350 fascinating mechanism, as it is possible that bacteria produce more exopolysaccharides in the  
351 attempt to compensate for the loss of flagella and its mechanical support. Also, if flagella indeed  
352 contribute to the biofilm's strength, future biofilm treatment approaches may potentially target  
353 flagella, to weaken the biofilm's structure and improve antibiotics penetration. Such a strategy  
354 may then be followed by an effective antibiotic treatment that would otherwise be less efficient  
355 in a strong and fully functional biofilm, and give way to future studies in clinical/environmental  
356 biofilms.

## 357 **Discussion**

358 The field of biofilm studies is of great importance for basic microbiological  
359 understanding as well as in medical applications. Being studied intensely for over 40 years there  
360 are still many pieces missing in the complex biofilm puzzle. Despite the vast interest, part of the  
361 reason for this great mystery is its complexity and the challenges in its manipulation. For the  
362 most part, biofilm research is performed through bulk population analysis<sup>15,37-39</sup>, resulting in the  
363 possibility of overlooking details that seem to be minor. It is likely that these details are those  
364 that are actually the crucial details for understanding the true nature and dynamics of the biofilm  
365 population. Direct evidence of factors from within the biofilm provides an important tool to  
366 tackle this challenge. The work presented here has focused on spatial and temporal localization  
367 of flagella in the biofilm, providing direct visualization for the first time.

368 A designated genetic code expansion system was developed for direct flagella labeling,  
369 enabling its direct identification and characterization in a mature biofilm. Following  
370 orthogonality establishment for the first time, this system was utilized for bio-tracking flagella  
371 inside biofilms. Direct imaging revealed inoculated flagella persistence during initial biofilm  
372 growth and maturation. It also revealed inoculated flagellar movement in the biofilm.  
373 Furthermore, as opposed to what was previously reported regarding flagella synthesis in a  
374 biofilm, we demonstrated that flagella are present in the biofilm throughout its entire lifecycle.  
375 While the presence of flagellated cells in compartments at the top of mushroom-like structures  
376 found in a grown biofilm are a common concept for dispersion of cells, we did not detect flagella  
377 any higher than the mid-section of these structures. Furthermore, we found that flagellated cells  
378 constantly left the biofilm, either carrying newly synthesized flagella or on rare occasions  
379 inoculated flagella. A combination of these findings led us to create an updated biofilm lifecycle  
380 model that includes the dynamics of flagella within these biofilms.

381 The unexpected discoveries regarding the presence of flagella inside the biofilm, led to a  
382 possible explanation for the reason behind this bacterial behavior with regards to the analysis of  
383 biofilm's physical strength. The detection of scaffold-like structures of flagella inside the biofilm  
384 resembled mechanical support needed for architectural buildings. This was strengthened when  
385 native biofilm displayed higher physical strength compared to a biofilm lacking flagella.  
386 Accordingly, we concluded that flagella play an important role in providing mechanical and  
387 physical support of the biofilm. Further research though is needed to clarify the exact details  
388 behind this newly suggested role of flagella in a biofilm setting. We do recognize the existing  
389 obstacles at play, however, the work presented herein strongly emphasizes the need for  
390 additional direct evidence of occurrences within the biofilm environment. Direct imaging can

391 thus serve as a window for new research venues. We posit that the new knowledge, afforded by  
392 this novel model, and approach that uses genetically code expanded strains as presented here will  
393 serve in tackling clinical/environmental biofilm research and envision multiple other new studies  
394 in regards to *P. aeruginosa*.

### 395 **Acknowledgments**

396 Prof. Ehud Banin is greatly acknowledged for useful discussions. We would like to thank  
397 the Ilse Katz Institute for Nanoscale Science and Technology Shred Resource Facility for their  
398 technical contribution in image acquisition with Zeiss LSM880 Airyscan (Dr. Uzi Hadad),  
399 Verios 460L Thermo Fisher Scientific HR-SEM (Einat Nativ-Roth), Helios G4 UC Thermo  
400 Fisher Scientific dual-beam HR-SEM (Nitzan Maman) and MFP-3D-Bio AFM (Juergen Jopp).  
401 Dr. Anna Bakhrat's assistance in genetic engineering is thankfully acknowledged. Yoni Ozer and  
402 Itay Algov's graphical assistance is thankfully acknowledged. Esti Kramarsky Winter is  
403 acknowledged for writing assistance. We thank the Kreitmann School for graduate students for a  
404 Ph.D. fellowship (E.O., A.B., K.Y.) and the Ben-Gurion University for a continued support of  
405 our research (L.A., A.K.).

### 406 **Contributions**

407 E.O. and K.Y. share equal contribution to this paper, E.O. conceived, performed and  
408 analyzed experimentations, established genetic code expansion system and authored the  
409 manuscript, K.Y. conceived, performed and analyzed all experimentations and co-authored the  
410 manuscript, E.C. performed nanoindentation experiments, A.B. synthesized unnatural amino  
411 acids used in this research, M.M.M., perceived and advised with *P. Aeruginosa* biofilm  
412 experiments, R.B. supervised, analyzed and wrote manuscript regarding AFM measurements,  
413 A.K. conceived experiments, supervised, provided research facilities and edited the manuscript,



414 L.A. conceived experiments, supervised the research, provided facilities, written and edited the  
415 manuscript.

416

## 417 **References**

- 418 1. Lee, K. & Yoon, S. S. Pseudomonas aeruginosa Biofilm, a Programmed Bacterial Life for  
419 Fitness. *J. Microbiol. Biotechnol.* **27**, 1053–1064 (2017).
- 420 2. Papenfort, K. & Bassler, B. L. Quorum sensing signal-response systems in Gram-negative  
421 bacteria. *Nat. Rev. Microbiol.* **14**, 576–588 (2016).
- 422 3. Høiby, N. A short history of microbial biofilms and biofilm infections. *Apmis* **125**, 272–  
423 275 (2017).
- 424 4. Parsek, M. R. & Greenberg, E. P. Sociomicrobiology: The connections between quorum  
425 sensing and biofilms. *Trends Microbiol.* **13**, 27–33 (2005).
- 426 5. Lappin-Scott, H., Burton, S. & Stoodley, P. Revealing a world of biofilms-the pioneering  
427 research of Bill Costerton. *Nat. Rev. Microbiol.* **12**, 781–787 (2014).
- 428 6. Maunders, E. & Welch, M. Matrix exopolysaccharides; the sticky side of biofilm  
429 formation. *FEMS Microbiol. Lett.* **364**, 1–10 (2017).
- 430 7. McDougald, D., Rice, S. A., Barraud, N., Steinberg, P. D. & Kjelleberg, S. Should we stay  
431 or should we go: Mechanisms and ecological consequences for biofilm dispersal. *Nat.*  
432 *Rev. Microbiol.* **10**, 39–50 (2012).
- 433 8. Petrova, O. E. & Sauer, K. Escaping the biofilm in more than one way: Desorption,  
434 detachment or dispersion. *Curr. Opin. Microbiol.* **30**, 67–78 (2016).
- 435 9. Barken, K. B. *et al.* Roles of type IV pili, flagellum-mediated motility and extracellular  
436 DNA in the formation of mature multicellular structures in Pseudomonas aeruginosa  
437 biofilms. *Environ. Microbiol.* **10**, 2331–2343 (2008).
- 438 10. Belas, R. Biofilms, flagella, and mechanosensing of surfaces by bacteria. *Trends*  
439 *Microbiol.* **22**, 517–527 (2014).
- 440 11. Blair, K. M., Turner, L., Winkelman, J. T., Berg, H. C. & Kearns, D. B. A molecular  
441 clutch disables flagella in the Bacillus subtilis biofilm. *Science (80-. ).* **320**, 1636–1638  
442 (2008).
- 443 12. Liu, X. *et al.* Flagella act as Geobacter biofilm scaffolds to stabilize biofilm and facilitate

- 444 extracellular electron transfer. *Biosens. Bioelectron.* **146**, 111748 (2019).
- 445 13. Klausen, M. *et al.* Biofilm formation by *Pseudomonas aeruginosa* wild type, flagella and  
446 type IV pili mutants. *Mol. Microbiol.* **48**, 1511–1524 (2003).
- 447 14. Tolker-Nielsen, T. *et al.* Development and dynamics of *Pseudomonas* sp. biofilms. *J.*  
448 *Bacteriol.* **182**, 6482–6489 (2000).
- 449 15. Whiteley, M. *et al.* Gene expression in *Pseudomonas aeruginosa* biofilms. *Nature* **413**,  
450 860–864 (2001).
- 451 16. Claudine, B. & Harwood, C. S. Cyclic diguanosine monophosphate represses bacterial  
452 flagella synthesis by interacting with the Walker a motif of the enhancer-binding protein  
453 FleQ. *Proc. Natl. Acad. Sci. U. S. A.* **110**, 18478–18483 (2013).
- 454 17. Lemke, E. a. The exploding genetic code. *ChemBioChem* vol. 15 1691–1694 (2014).
- 455 18. Cohen, M., Ozer, E., Kushmaro, A. & Alfonta, L. Cellular localization of cytochrome bd  
456 in cyanobacteria using genetic code expansion. *Biotechnol. Bioeng.* **117**, 523–530 (2020).
- 457 19. Aloush, N. *et al.* Live Cell Imaging of Bioorthogonally Labelled Proteins Generated With  
458 a Single Pyrrolysine tRNA Gene. *Sci. Rep.* **8**, 14527 (2018).
- 459 20. Kipper, K. *et al.* Application of Noncanonical Amino Acids for Protein Labeling in a  
460 Genomically Recoded *Escherichia coli*. *ACS Synth. Biol.* **6**, 233–255 (2017).
- 461 21. Zhang, J. *et al.* Small Unnatural Amino Acid Carried Raman Tag for Molecular Imaging  
462 of Genetically Targeted Proteins. *J. Phys. Chem. Lett.* **9**, 4679–4685 (2018).
- 463 22. Chemla, Y. *et al.* Expanding the Genetic Code of a Photoautotrophic Organism.  
464 *Biochemistry* **56**, 2161–2165 (2017).
- 465 23. Gan, Q., Lehman, B. P., Bobik, T. A. & Fan, C. Expanding the genetic code of *Salmonella*  
466 with non-canonical amino acids. *Sci. Rep.* **6**, 39920–39926 (2016).
- 467 24. Bianco, A., Townsley, F. M., Greiss, S., Lang, K. & Chin, J. W. Expanding the genetic  
468 code of *Drosophila melanogaster*. *Nat. Chem. Biol.* **8**, 748–750 (2012).
- 469 25. Ernst, R. J. *et al.* Genetic code expansion in the mouse brain. *Nat. Chem. Biol.* **12**, 776–  
470 778 (2016).
- 471 26. Cervettini, D. *et al.* Rapid discovery and evolution of orthogonal aminoacyl-tRNA  
472 synthetase–tRNA pairs. *Nat. Biotechnol.* **38**, 989–999 (2020).
- 473 27. Ozer, E. *et al.* In vitro suppression of two different stop codons. *Biotechnol. Bioeng.* **114**,  
474 1065–1073 (2017).

- 475 28. Nakamura, Y. Codon usage tabulated from international DNA sequence databases: status  
476 for the year 2000. *Nucleic Acids Res.* **28**, 292–292 (2000).
- 477 29. Singh, M. S., Chowdhury, S. & Koley, S. Advances of azide-alkyne cycloaddition-click  
478 chemistry over the recent decade. *Tetrahedron* **72**, 5257–5283 (2016).
- 479 30. Chemla, Y., Ozer, E., Algov, I. & Alfonta, L. Context effects of genetic code expansion  
480 by stop codon suppression. *Curr. Opin. Chem. Biol.* **46**, 146–155 (2018).
- 481 31. Chaban, B., Hughes, H. V. & Beeby, M. The flagellum in bacterial pathogens: For  
482 motility and a whole lot more. *Semin. Cell Dev. Biol.* **46**, 91–103 (2015).
- 483 32. Minamino, T. & Namba, K. Self-assembly and type III protein export of the bacterial  
484 flagellum. *J. Mol. Microbiol. Biotechnol.* **7**, 5–17 (2004).
- 485 33. Schlesinger, O. *et al.* Tuning of Recombinant Protein Expression in Escherichia coli by  
486 Manipulating Transcription, Translation Initiation Rates, and Incorporation of  
487 Noncanonical Amino Acids. *ACS Synth. Biol.* **6**, 1076–1085 (2017).
- 488 34. Watnick, P. & Kolter, R. Biofilm , City of Microbes. **182**, 2675–2679 (2000).
- 489 35. Stoodley, P., Sauer, K., Davies, D. G. & Costerton, J. W. Biofilms as Complex  
490 Differentiated Communities. *Annu. Rev. Microbiol.* **56**, 187–209 (2002).
- 491 36. Sauer, K. *et al.* Pseudomonas aeruginosa Displays Multiple Phenotypes during  
492 Development as a Biofilm. *J. Bacteriol.* **184**, 1140–1154 (2002).
- 493 37. Schniederberend, M. *et al.* Modulation of flagellar rotation in surfaceattached bacteria: A  
494 pathway for rapid surface-sensing after flagellar attachment. *PLoS Pathog.* **15**, 1–30  
495 (2019).
- 496 38. Morgan, R., Kohn, S., Hwang, S. H., Hassett, D. J. & Sauer, K. BdlA, a chemotaxis  
497 regulator essential for biofilm dispersion in Pseudomonas aeruginosa. *J. Bacteriol.* **188**,  
498 7335–7343 (2006).
- 499 39. Tart, A. H., Wolfgang, M. C. & Wozniak, D. J. The Alternative Sigma Factor AlgT  
500 Represses Pseudomonas aeruginosa Flagellum Biosynthesis by Inhibiting Expression of  
501 fleQ. *J. Bacteriol.* **187**, 7955–7962 (2005).
- 502 40. Wu, H., Moser, C., Wang, H. Z., Høiby, N. & Song, Z. J. Strategies for combating  
503 bacterial biofilm infections. *Int. J. Oral Sci.* **7**, 1–7 (2015).
- 504 41. Zhao, K., Liu, M. & Burgess, R. R. Adaptation in bacterial flagellar and motility systems:  
505 From regulon members to 'foraging'-like behavior in E. coli. *Nucleic Acids Res.* **35**,

- 506 4441–4452 (2007).
- 507 42. Serra, D. O., Richter, A. M., Klauck, G., Mika, F. & Hengge, R. Microanatomy at Cellular  
508 Resolution and Spatial Order of Physiological Differentiation in a Bacterial Biofilm. *MBio*  
509 **4**, 1–12 (2013).
- 510 43. Chen, W. *et al.* CRISPR/Cas9-based Genome Editing in *Pseudomonas aeruginosa* and  
511 Cytidine Deaminase-Mediated Base Editing in *Pseudomonas* Species. *iScience* **6**, 222–231  
512 (2018).
- 513 44. Tallawi, M., Opitz, M. & Lieleg, O. Modulation of the mechanical properties of bacterial  
514 biofilms in response to environmental challenges. *Biomater. Sci.* **5**, 887–900 (2017).
- 515 45. Baniyadi, M. *et al.* Nanoindentation of *Pseudomonas aeruginosa* bacterial biofilm using  
516 atomic force microscopy. *Mater. Res. Express* **1**, 045411 (2014).
- 517 46. Zeng, G. *et al.* Functional bacterial amyloid increases *Pseudomonas* biofilm  
518 hydrophobicity and stiffness. *Front. Microbiol.* **6**, 1–14 (2015).
- 519 47. Harrison, J. J. *et al.* Elevated exopolysaccharide levels in *Pseudomonas aeruginosa* flagellar  
520 mutants have implications for biofilm growth and chronic infections. *PLOS Genet.* **16**,  
521 e1008848 (2020).
- 522

523 **Online Methods**

524 ***Reagents***

525 PrK ((S)-2-Amino-6-((prop-2-ynoxy)carbonylamino)hexanoic acid) and AzCK ((S)-2-  
526 Amino-6-((2-azidoethoxy)carbonylamino)hexanoic acid) were both synthesized according to a  
527 protocol reported by Nguyen et al.<sup>48</sup>. Tris(3-hydroxypropyltriazolylmethyl)amine (THPTA),  
528 Tetramethylrhodamine-azide and Tetramethylrhodamine-alkyne were purchased from Sigma-  
529 Aldrich (Rehovot, Israel). MB 660R Azide was a kind donation from Click Chemistry Tools  
530 (Scottsdale, AZ, USA). All restriction enzymes were purchased from Thermo Fisher Scientific  
531 (Waltham, MA, USA), while all DNA oligonucleotides were obtained from Syntezza Bioscience  
532 (Jerusalem, Israel).

533 ***Plasmids construction***

534 All plasmids for initial method establishment were constructed by a standard yeast assembly  
535 protocol<sup>22</sup>. The upstream and downstream regions from *P. aeruginosa*'s leucyl translational  
536 system were chosen for OTS expression. Upstream and downstream regions of leucyl tRNA  
537 "flanked" pyrrolysyl tRNA, as well as for the upstream and downstream regions of leucyl tRNA-  
538 synthetase that "flanked" pyrrolysyl tRNA-synthetase. The deGFP reporter gene (a variant  
539 designed for better expression in in-vitro systems, but also works well in in-vivo systems) was  
540 also chosen to have a PAO1 endogenous promoter, the flagellin native promoter (*fliC* promoter).  
541 It was chosen considering *fliC* gene was designed for Uaa incorporation after deGFP.

542 The initial construct (pPaGE Pyl TAG *fliC* prom deGFP WT NHis) was assembled in two  
543 stages. First, pMRP9-1 backbone was amplified using primers 1 and 2 (table S1), without the  
544 deGFP gene, and was assembled with the 2 $\mu$  origin and URA3 selectivity gene for yeast.  
545 Second, the new vector after restriction with BamHI was assembled with seven other PCR

546 amplified parts, containing the OTS, deGFP expression gene and necessary promoters and  
547 terminators (primers 3-16, table S1). Endogenous regions of *P. aeruginosa* were amplified from  
548 PAO1 genome. N-terminal his-tag deGFP and its T500 terminator were amplified from the  
549 pBEST plasmid<sup>27</sup>. Pyrrolysyl tRNA-synthetase was amplified from pEVOL-Pyl plasmid  
550 described in previous work<sup>27</sup>. Pyrrolysyl tRNA was assembled through primers 4 and 5  
551 homology (table S1) during the yeast assembly. The pPaGE Pyl TAG *fliC* prom deGFP  
552 Y35TAG NHis construct was assembled in the same manner, only with a mutant deGFP  
553 amplified from the pBEST plasmid.

554 Variant for orthogonality testing of Pyl tRNA was generated through standard DNA collapse  
555 using HindIII. HindIII restriction, followed by self-ligation of the plasmid without the PylRS  
556 gene. During the initial construct generation, a deletion construct without Pyl tRNA was also  
557 created. This variant was used for orthogonality testing of PylRS.

558 A construct containing the *fliC* gene with a TAG mutation (pPaGE Pyl TAG *fliC* T248TAG)  
559 was assembled through Gibson assembly. pPaGE was restricted with NcoI for vector generation  
560 without the deGFP gene and T500 terminator. *fliC* gene had the TAG mutation installation as  
561 part of the assembly, by two pieces amplification. The gene, together with its downstream  
562 sequence, was amplified from the PAO1 genome using primers 17+20 and 19+18 (table S1).

563 All plasmids inserted into *E. coli* underwent standard heat-shock transformation protocol.

564 All plasmids inserted into *P. aeruginosa* underwent standard electroporation protocol.

### 565 ***Viability assay***

566 Bacterial liquid culture in LB-Miller, after 24 hrs of growth at 37°C, was diluted 1:100. The  
567 diluted culture was placed at 37°C. Every 1 hr, a duplicate was measured for OD at a wavelength  
568 of 600 nm using a Synergy HT plate reader (Biotek, Winooski, VT, USA). After 17 hrs of

569 measurements, when the cells reached growth plateau, the culture was left for incubation for  
570 another 10 hrs, when a final measurement was taken. When needed, the culture was  
571 supplemented with final concentration of 1 mM Uaa (optimal concentration found is shown in  
572 Fig S36). In case of plasmid containing bacteria, growth medium was supplemented with 300  
573  $\mu\text{g}/\text{mL}$  carbenicillin.

#### 574 ***Suppression efficiency***

575 Five separate sets of liquid cultures were grown at  $37^{\circ}\text{C}$  for 24 hrs. Each set was tested for  
576 GFP expression and was composed of a native strain of *P. aeruginosa*, WT GFP and Y35TAG  
577 GFP with PrK. Following growth, each sample, from each set, was tested in triplicates for OD at  
578 a wavelength of 600 nm and GFP fluorescence by using a Synergy HT plate reader (Biotek,  
579 Winooski, VT, USA). Each sample's fluorescence was divided by the  $\text{OD}_{[600]}$  value. Values of  
580 WT and Y35TAG with PrK were normalized to the native strain's value of fluorescence/ $\text{OD}_{[600]}$ .  
581 Finally, the suppression efficiency of each set was determined through value of normalized  
582 fluorescence/ $\text{OD}_{[600]}$  of mutant divided by the value of normalized fluorescence/ $\text{OD}_{[600]}$  of WT.

583 Error bar in figure 1e could only be calculated for mutant expression (as WT is always 100%  
584 by definition), representing the standard deviation between 5 different suppression efficiencies  
585 values calculated.

#### 586 ***Protein expression in PAO1 and cells lysis***

587 Culture growth: PAO1 harboring pPaGE variants, were grown in LB-Miller with 300  $\mu\text{g}/\text{mL}$   
588 carbenicillin at  $37^{\circ}\text{C}$  for 24 hrs. After growth, the cultures were diluted 1:100 for another 24 hrs  
589 of growth. In case of needed Uaa addition, the culture was supplemented with final concentration  
590 of 1 mM Uaa.

591 Lysis: Following 24 hrs of growth, 1 mL of culture was sedimented and resuspended with 1  
592 mL of phosphate buffer 100 mM pH 7. The cells were once again sedimented and were  
593 resuspended with 100  $\mu$ L lysis solution composed of: 90% phosphate buffer, 10% BugBuster®  
594 10X protein extraction reagent (Merck, Billerica, MA, USA), Turbonuclease (Sigma, St. Louis,  
595 MO, USA), Lysozyme (Sigma-Aldrich, Rehovot, Israel) and protease inhibitor (Merck,  
596 Darmstadt, Germany). Cells were incubated with the lysis solution for 30 min at room  
597 temperature while shaking, followed by 4°C centrifugation at 10000 g for 10 min. Supernatant  
598 containing soluble proteins fraction was taken for further analysis.

599 ***Click reaction followed by SDS-PAGE, fluorescent imaging and Western-blot analysis***

600 Cu(I)-catalyzed azide-alkyne cycloaddition (CuAAC) click reaction<sup>29</sup> was performed on  
601 lysates at a final volume of 50  $\mu$ L. A fluorophore (with either an azide moiety or an alkyne  
602 moiety, according to necessity) was added to a concentration of 50  $\mu$ M, while THPTA, sodium  
603 ascorbate and CuCl<sub>2</sub> were added to final concentration of 1.2 mM, 2.5 mM and 200  $\mu$ M,  
604 respectively. A volume of 20  $\mu$ L of cell lysate was added to the reaction, followed by 1 hr  
605 incubation at room temperature with shaking. Clicked samples were examined through SDS-  
606 PAGE 4-20% Expressplus protein gel (GenScript, Nanjing, China). Fluorescent SDS-PAGE  
607 images were obtained through ImageQuant LAS 4000 imager (Fujifilm, Tokyo, Japan), using  
608 green light (520 nm Epi) and a 575 nm Cy3 detection filter. Next, when Western-blot was  
609 needed, SDS-PAGE was transferred to a membrane (Bio-Rad, Hercules, CA, USA) through  
610 eBlot® protein transfer system (GenScript, Nanjing, China). Using goat T-19 anti GFP  
611 antibody<sup>49</sup> (sc-5384, Santa Cruz, CA, USA) as a primary antibody and donkey anti goat IgG-  
612 HRP<sup>50</sup> (sc-2020, Santa Cruz, CA, USA) as a secondary antibody, standard Western-blot protocol



613 was performed. Chemiluminescence imaging was done using ImageQuant LAS 4000 imager  
614 (Fujifilm, Tokyo, Japan).

#### 615 ***Protein purification and mass spectrometry***

616 A 200 mL culture of the *P. aeruginosa* GFP Y35TAG mutant, in the presence of PrK, was  
617 grown at 37°C for 24 hrs. Using standard needle sonication, culture was lysed and purified using  
618 IMAC (Novagene, Madison, WI, USA) according to manufacturer guidelines. Elution fraction  
619 was concentrated using Vivaspin 6, 10000 MWCO PES (Sartorius, Goettingen, Germany) and  
620 concentrated fraction was analyzed by liquid chromatography mass spectrometry (LCMS)  
621 (Finnigan Surveyor Autosampler Plus/LCQ Fleet, Thermo Scientific, Waltham, MA, USA).

#### 622 ***Theoretical model of P. aeruginosa flagella***

623 A monomer model of *P. aeruginosa* flagellin was obtained through SWISS-MODEL<sup>51</sup> and a  
624 PrK residue was incorporated in position 248 (PyMOL Molecular Graphics System, Version 2.0  
625 Schrödinger, LLC). PDB file 5WK5, containing 41 subunits of the *P. aeruginosa*'s filament core  
626 (no outer protein structure of D2 and/or D3), was used as alignment reference for 41 SWISS-  
627 MODEL generated monomers with PrK (PyMOL Molecular Graphics System, Version 2.0  
628 Schrödinger, LLC). The final product is a theoretical model of a flagella filament, consisting of  
629 41 *P. aeruginosa* flagellin proteins, all of which contain PrK in the 248<sup>th</sup> position.

#### 630 ***Live-cell click reaction and flow-cells construction***

631 pPaGE harboring *fliC* with TAG mutation at the 248<sup>th</sup> site, was electroporated into PAO1  
632 gGFP strain (a strain containing GFP expression gene in the genome, gGFP = genome GFP).  
633 Liquid culture in the presence of PrK, was grown at 37°C for 24 hrs. Grown culture at the  
634 volume of 200 µL was centrifuged and resuspended with 20 µL phosphate buffer 100 mM pH 7.  
635 Click reagents were added to a final reaction volume of 50 µL. Azide-containing 545

636 fluorophore was added to a concentration of 50  $\mu\text{M}$ , while THPTA, sodium ascorbate and  $\text{CuCl}_2$   
637 were added to a final concentration of 1.2 mM, 2.5 mM and 200  $\mu\text{M}$ , respectively. Following 40  
638 min incubation at room temperature with shaking, cells were washed three times with 1 mL of  
639 phosphate buffer 100 mM pH 7 and were brought to a value of  $\text{OD}_{600}$  of 0.1. A flow-cell system  
640 was constructed as described before<sup>52</sup>, using the labeled bacteria as inoculation for growth.  
641 Following 1 hr of static attachment in the flow-cell at 30°C, AB minimal growth media at  
642 temperature of 37°C was supplied at a rate of 4 mL/hr. Flow-cells were grown for up to 6 days  
643 while imaging for different experimental procedures was done using confocal laser scanning  
644 microscopy (CLSM).

645 For pre-inoculation labeled flagella tracking –flow-cell was constructed as described and was  
646 imaged using CLSM at 2 different channels (488 at cyan for bacteria and 545 at magenta for pre-  
647 inoculation labeled flagella) at specific locations every several hours for up to 6 days.

648 For effluent flagella tracking –flow-cell was constructed as described while AB minimal  
649 media was supplemented with PrK for continuous incorporation. Effluent of ~15 mL was  
650 collected into ice following 2/4/6 days of growth. Effluent total volume was pelleted down and  
651 resuspended with 20  $\mu\text{L}$  phosphate buffer 100 mM pH 7. Click reagents were added to a final  
652 reaction volume of 50  $\mu\text{L}$ . Azide-containing 660 fluorophore was added to a concentration of 50  
653  $\mu\text{M}$ , while THPTA, sodium ascorbate and  $\text{CuCl}_2$  were added to a final concentration of 1.2 mM,  
654 2.5 mM and 200  $\mu\text{M}$ , respectively. Following 40 min incubation at room temperature with  
655 shaking, cells were washed two times with 1 mL of phosphate buffer 100 mM pH 7 and were  
656 finally resuspended with ~50  $\mu\text{L}$  PB 100 mM pH 7. Labeled effluent (5  $\mu\text{L}$  onto a glass slide)  
657 was imaged using CLSM at 3 different channels (488 at cyan for bacteria, 545 at magenta for  
658 pre-inoculation labeled flagella, 660 at orange for newly synthesized labeled flagella).

659 For newly synthesized labeled flagella tracking within a biofilm – flow-cell was constructed  
660 as described and grown for 2/4/6 days while AB minimal media was supplemented with PrK for  
661 continuous incorporation. Click reagents solution was prepared for a final reaction volume of  
662 500  $\mu$ L. Azide-containing 545 fluorophore was added to a concentration of 50  $\mu$ M, while  
663 THPTA, sodium ascorbate and  $\text{CuCl}_2$  were added to a final concentration of 1.2 mM, 2.5 mM  
664 and 200  $\mu$ M, respectively. The click mixture was slowly injected into the flow-cell chamber and  
665 remained stationary for 20 min at room temperature, followed by intensive wash with growth  
666 media at a rate of 16 mL/hr at room temperature. Flow-cell was imaged using CLSM at 2  
667 different channels (488 at cyan for bacteria, 545 at magenta for labeled flagella).

668 All mentioned experimental procedures were repeated for a minimum number of 5 different  
669 flow-cells.

#### 670 *Confocal microscope settings and image analysis*

671 Confocal images were acquired using Zeiss LSM880 system (Zena, Germany). Plan-  
672 Apochromat 63x/1.4 Oil DIC M27 or Plan-Apochromat 40x/1.3 Oil DIC M27 objective were  
673 used. Cyan channel was imaged using 488 nm Argon laser (usually in the range of 5-15%) with  
674 emission filter BP 493-556. Magenta channel was imaged using 561 nm DPSS laser (usually in  
675 the range of 2-4%) with emission filter BP 570-624. Orange channel was imaged using 633 nm  
676 HeNe laser (usually in the range of 8-15%) with emission filter BP 638-755.

677 Scanning resolution for all flow-cells was 1024x1024. Scanning resolution for effluent  
678 planktonic cells was 2048x2048.

679 Image analysis was performed using either ImageJ software (National institutes of health,  
680 USA) or IMARIS software (Bitplane AG, Zurich, Switzerland). Despite channel modifications in  
681 image analysis, a gamma value of 1.00 was strictly conserved in all images and analysis.

682 Figure 2b – all 9 Z plains were stacked and channels were merged (488+545) and a smooth  
683 filter was used. (ImageJ)

684 Figures 2d – 3D digital visualization of 545 alone or merged channels (488+545) were at  
685 6000x6000 dimensions and 900 dpi using “shadow” function. (IMARIS)

686 Figure 2e – Out of 118 Z plains, 61-65 were stacked and 488+545 channels were merged.  
687 (ImageJ)

688 Figures 3b –Digital bio-volume was saved as 6000x6000 and 900 dpi. 2 days mid-section  
689 was stacked from 13-16 Z plains. Upper-section was stacked from 20-25 Z plains. Lower mid-  
690 section was stacked from 27-39 Z plains. Mid-section was stacked from 66-68 Z plains.  
691 (IMARIS)

692 Figures 4b – Out of 13 Z plains, image was stacked using 4-9 Z plains and saved as  
693 individual channels (488/545/660) or a merged image of all channels. (ImageJ)

694 Figure 6a – The 14 Z plain was presented only in the 545 channel. (IMARIS)

695 Figure 6b – Z plains of 23-26 were stacked and saved as individual 545 channel or a merged  
696 image of 488+545. (IMARIS)

### 697 ***P. aeruginosa PAO1 gGFP ΔfliC strain generation***

698 For the creation of a KO strain to flagella filament, a CRISPR/Cas9-based platform adapted  
699 to *P. aeruginosa*<sup>43</sup> was utilized. Out of a 2-plasmids system, pCasPA plasmid was used as is,  
700 while a relevant pACRISPR plasmid had to be constructed using Gibson assembly to contain  
701 gRNA and complementary homology region to the genome. The gRNA used was chosen based  
702 on CHOPCHOP<sup>53</sup> and complemented sites 168-174 in *fliC* gene. Homology region was chosen  
703 as 500 bp upstream to the ATG codon of *fliC*, 30 bp from the end of the *fliC* gene (including  
704 stop-codon) and 500 bp downstream to the stop-codon of *fliC*, meaning deletion of 1437 bp out

705 of the *fliC* gene. Gibson assembly for pACRISPR with relevant gRNA and homology was done  
706 using primers 21-28 (table S1), following standard assembly and plasmid sequence verification.  
707 pCasPA was electroporated into PAO1 gGFP strain using standard protocol and grown on  
708 tetracycline 100 µg/mL selective plate. After first plasmid insertion, PAO1 gGFP pCasPA was  
709 grown over night at 37°C, and was added with L-arabinose to final concentration of 2 mg/mL for  
710 2 hrs incubation at 37°C (targeted for Cas9 inductive protein expression). Cells then were  
711 prepared for electroporation using standard protocol. pACRISPR targeted for *fliC* deletion was  
712 electroporated into PAO1 gGFP pCasPA cells prepared in advance and grown on tetracycline  
713 100 µg/mL + carbenicillin 150 µg/mL. Colonies were screened for genome segment  
714 modification and chosen colonies were cured from both plasmids by plating on sucrose 5%  
715 plates. Chosen colony was isolated, tested for positive plasmid curing, and tested by PCR for  
716 positive deletion (primers 29+30, table S1). PCR segment was purified using nucleospin gel and  
717 PCR clean-up (MACHEREY-NAGEL, Germany) and underwent Sanger sequencing with primer  
718 31 (table S1).

#### 719 ***WT/KO strains flow-cells construction***

720 WT (PAO1 gGFP) or KO (PAO1 gGFP  $\Delta$ *fliC*) strain stationary grown liquid culture was  
721 diluted to OD<sub>600</sub> of 0.1 and cells were inoculated in a flow-cell as described before. After 1 hr of  
722 attachment at 30°C, 37°C heated AB minimal media at a rate of 4 mL/hr was supplemented for 5  
723 days of growth. Flow-cells were examined for biofilm structure and 3D maturation using CLSM.

#### 724 ***Transmission electron microscopy (TEM)***

725 Grown bacteria cultures were diluted 1:20. A carbon type-B TEM grid was prepared using  
726 plasma cleaner PDC-32G (HARRICK PLASMA, Ithaca, NY, USA) for 30 sec. TEM grids were  
727 loaded with 2 µL from the diluted liquid culture, while excess liquid was dried using filter paper.

728 Prepared grids were examined in FEI Tecnai T12 G2 TWIN transmission electron microscope  
729 operating at 120 kV.

### 730 ***Swarming assay***

731 *P. aeruginosa* PA01 were grown overnight in LB-Miller medium. The next day, the bacteria  
732 were diluted 1:100 into fresh M9 medium and were grown to mid-log phase. The swarming  
733 plates were prepared using M9, solidified with 0.7% [wt/vol] Difco agar. Following bacteria  
734 refreshment, 2  $\mu$ L of the inoculums were placed in the middle of the plates enabling assessment  
735 of surface coverage after 24 hrs of growth at 37°C.

### 736 ***Static biofilm growth***

737 Round glass coverslips, 15 mm diameter (Ted Pella, Inc., Redding, CA, USA) were  
738 incubated with HCl 8% for 1 hr at room temperature and underwent autoclave sterilization in  
739 advance to biofilm growth. WT (PAO1 gGFP) or KO (PAO1 gGFP  $\Delta$ *fliC*) were refreshed by  
740 taking 30  $\mu$ L stationary grown culture into 3 mL LB-Miller for 3 hrs at 37°C with agitation.  
741 Reaching an OD<sub>600</sub> of ~0.2, 20  $\mu$ L of refreshed culture were taken into 2 mL of LB-Lenox in a  
742 12-well plate's well. Treated glass cover slip was placed in the well as well. Plate was incubated  
743 at 37°C for 16 hrs. Wells surrounding sample, were filled with DDW to keep high moisture  
744 during growth.

### 745 ***High-resolution scanning electron microscopy (HR-SEM)***

746 Following static biofilm growth, liquid was aspirated and the glass cover slip underwent  
747 fixation (2.5% glutaraldehyde, 2% paraformaldehyde, 0.2 M phosphate buffer) for 15 min.  
748 Samples were washed twice with PBS, 10 min each time, and were dehydrated using increasing  
749 ethanol concentrations before an addition of hexamethyldisilazane/ethanol solution in increasing  
750 concentrations. Finally, all liquids were removed and samples were dried in a chemical hood.

751 Fixed glasses were coated in Cr using Quorum Q150T-ES sputter and examined in Verios 460L  
752 Thermo Fisher Scientific scanning electron microscope operating at 3.00 kV.

### 753 ***Dual-beam HR-SEM***

754 For an inside look at a biofilm and not just outer-rim observations, the same glasses coated  
755 with Cr that were used for HR-SEM, were also analyzed with dual-beam HR-SEM. Areas meant  
756 for examination were locally coated with Pt and were sliced using focused ion beam. Biofilm's  
757 inside was examined in Helios G4 UC Thermo Fisher Scientific scanning electron microscope  
758 operating at 5.00 kV.

759

### 760 ***Atomic force microscopy (AFM) imaging***

761 Following static biofilm growth, the well was washed twice with PBS and left to dry in a  
762 hood. The dry samples were imaged on a MFP-3D-Bio (Oxford Instruments Asylum Research,  
763 Santa Barbara, CA, USA) in AC-mode ("tapping mode") in air, using an AC240BSA probe  
764 (Olympus) at room temperature. Imaging rate was of 0.5 Hz, with parameters of 512 scan lines  
765 and 1024 scan points.

### 766 ***AFM nanoindentation***

767 Local stiffness modulus,  $K$ , of the two different biofilms was measured with nano-indentation  
768 experiments performed on a Luigs & Neurann LTD AFM. The biofilm samples were grown on a  
769 clean glass coverslip as was mentioned before. The grown biofilm on top the coverslip was  
770 gently washed with PBS and semi-dried in open air. The indentation was performed with  
771 pyramidal silicon nitride cantilevers (V-shape MLCT, Bruker) with a measured mean spring  
772 constant of 0.01 N/m. The normal spring constants of the cantilevers were determined before  
773 each measurement using the equipartition theorem<sup>54</sup>. In a nano-indentation measurement, force-

774 distance curves are collected by approaching the cantilever tip towards the surface of the biofilm  
775 sample at a rate of 400 nm/s and indentation depth amplitude of 500 nm. Corresponding to the  
776 compliance of the sample, the cantilever deflects proportionally to the compliance of the sample.  
777 The curvature of this response region was fitted using the Sneddon model<sup>55,56</sup>, a contact  
778 mechanics model for a conical sharp probe (as the one used), to the force distance curves:

$$F = \frac{K}{1 - \nu^2} \left( \frac{2}{\pi} \right) \tan(\alpha) \delta^2$$

779 where  $\nu$  is Poisson ratio, taken as 0.5 (typical value for incompressible materials),  $\delta$  is the  
780 indentation length coordinate,  $\theta$  is the cone half angle (face angle) of the AFM probe, taken as  
781 the manufacturer's nominal value of 29.1°, and  $K$  is the local stiffness modulus. The indentation  
782 was performed at random locations across the surface of each biofilm sample. The measurement  
783 sets were repeated three times for each biofilm sample, where each set was comprised of 100  
784 force-distance traces. All measurements were carried out under PBS buffer (150 mM NaCl, 20  
785 mM PBS, pH 7.2) at room temperature. All data were recorded and analyzed using custom  
786 software written in Igor Pro 6.37 (Wavemetrics).

787 From 100 collected values of  $K$  for each biofilm, we constructed their probability  
788 distributions, and fitted them with the relevant statistical model. The Freedman-Diaconis rule  
789 was used as criterion for setting the bin size of the distributions<sup>57</sup>. The stiffness distribution of  
790 the WT biofilm was fitted with a Gaussian distribution,  $\phi(K) = (\sigma(2\pi)^{1/2})^{-1} \exp\{-1/2[(K - \mu)/\sigma]^2\}$ ,  
791 and the stiffness distribution of the  $\Delta$ *fliC* biofilm was fitted with the Gamma distribution, which  
792 is given by  $\phi(K) = (\beta^\alpha/\Gamma(\alpha))K^{\alpha-1}e^{-\beta K}$ . This latter is highly useful to describe the distribution of a  
793 random variable that does not normally distribute. The mean is calculated by  $\mu$  and  $\alpha/\beta$  (for the  
794 normal and Gamma distributions respectively) and the variance (from which the standard



795 deviation is calculated by taking its root) by  $\sigma^2$  and  $\alpha/\beta^2$  (for the normal and Gamma distributions  
796 respectively).

797

#### 798 **Additional references for online methods**

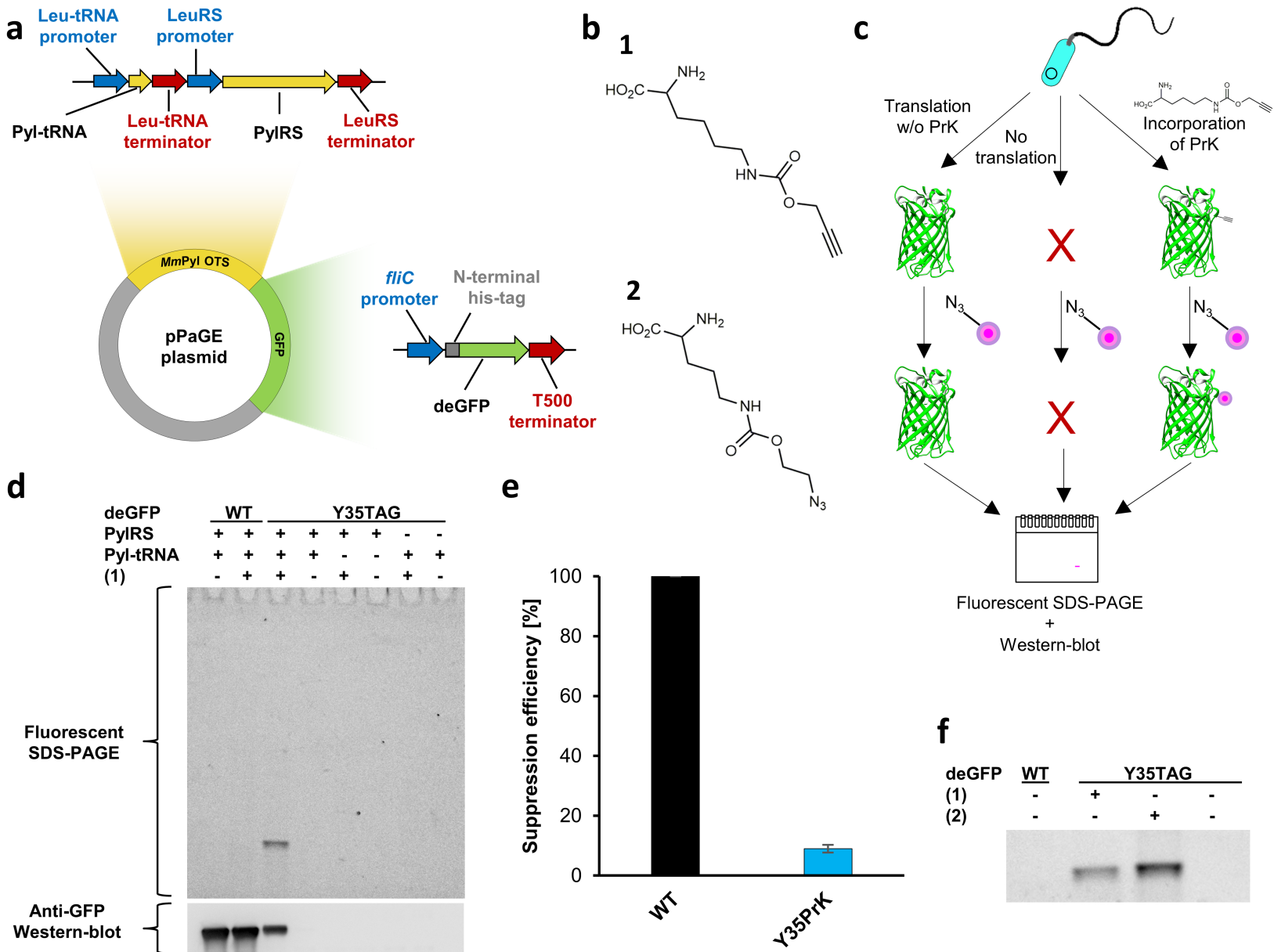
- 799 48. Nguyen, D. P. *et al.* Genetic Encoding and Labeling of Aliphatic Azides and Alkynes in  
800 Recombinant Proteins via a Pyrrolysyl-tRNA Synthetase/tRNA CUA Pair and Click  
801 Chemistry. *J. Am. Chem. Soc.* **131**, 8720–8721 (2009).
- 802 49. Ketema, M. *et al.* The rod domain is not essential for the function of plectin in  
803 maintaining tissue integrity. *Mol. Biol. Cell* **26**, 2402–2417 (2015).
- 804 50. Dunphy, G. *et al.* Non-canonical Activation of the DNA Sensing Adaptor STING by  
805 ATM and IFI16 Mediates NF- $\kappa$ B Signaling after Nuclear DNA Damage. *Mol. Cell* **71**,  
806 745–760 (2018).
- 807 51. Waterhouse, A. *et al.* SWISS-MODEL: homology modelling of protein structures and  
808 complexes. *Nucleic Acids Res.* **46**, W296–W303 (2018).
- 809 52. Yaniv, K. *et al.* Functional marine metagenomic screening for anti-quorum sensing and  
810 anti-biofilm activity. *Biofouling* **33**, 1–13 (2017).
- 811 53. Labun, K. *et al.* CHOPCHOP v3: Expanding the CRISPR web toolbox beyond genome  
812 editing. *Nucleic Acids Res.* **47**, W171–W174 (2019).
- 813 54. Hutter, J. L. & Bechhoefer, J. Calibration of atomic-force microscope tips. *Rev. Sci.*  
814 *Instrum.* **64**, 1868–1873 (1993).
- 815 55. Sneddon, I. N. The relation between load and penetration in the axisymmetric boussinesq  
816 problem for a punch of arbitrary profile. *Int. J. Eng. Sci.* **3**, 47–57 (1965).
- 817 56. Krieg, M. *et al.* Atomic force microscopy-based mechanobiology. *Nat. Rev. Phys.* **1**, 41–

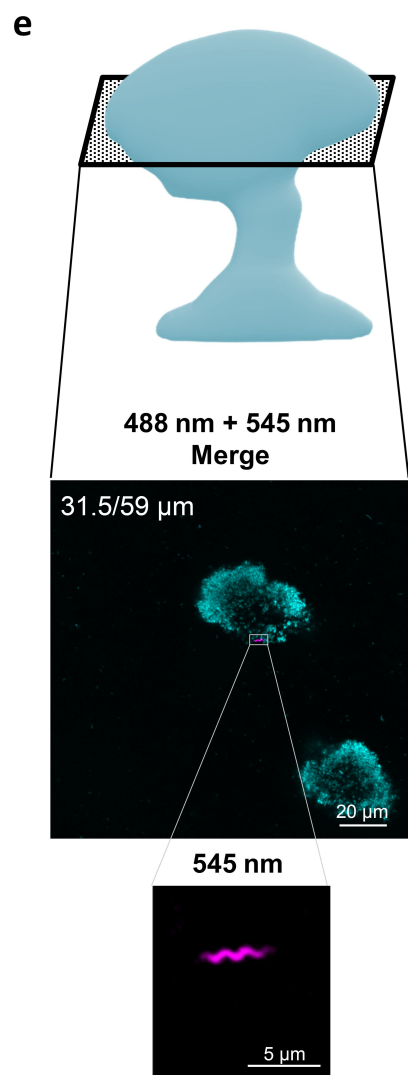
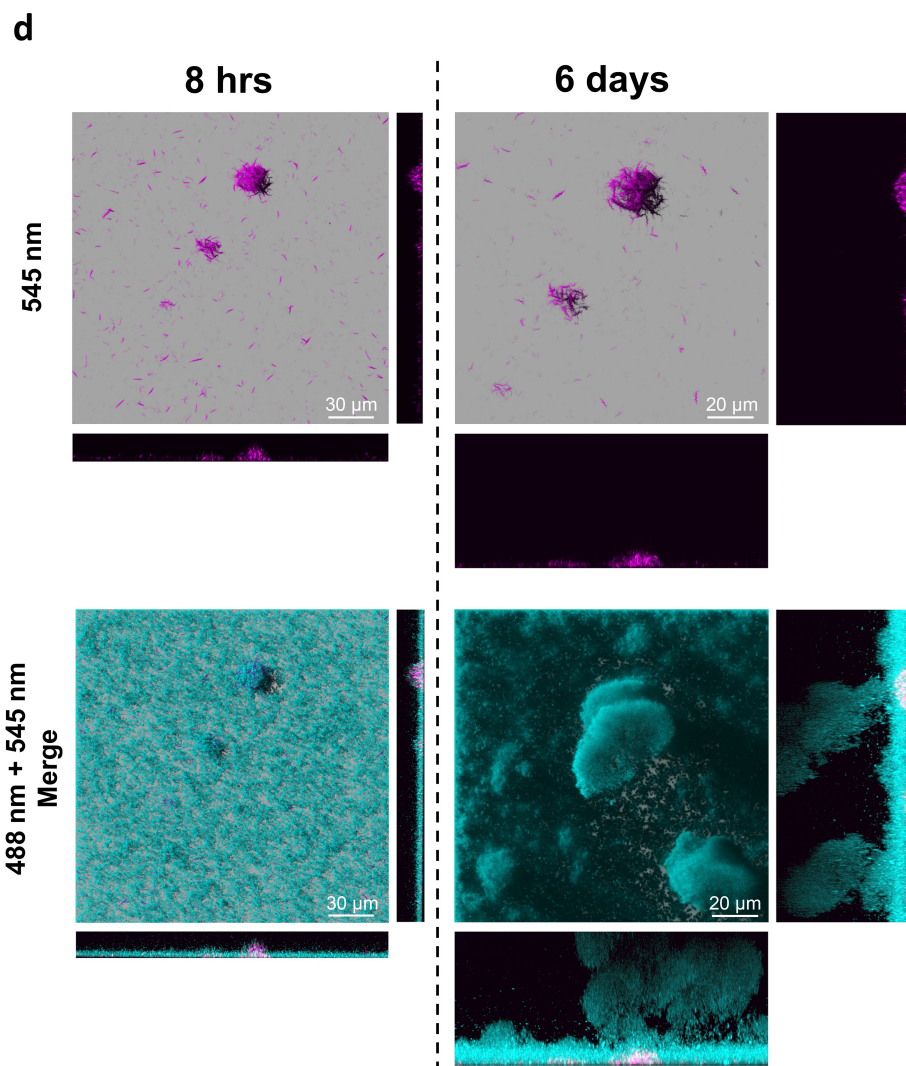
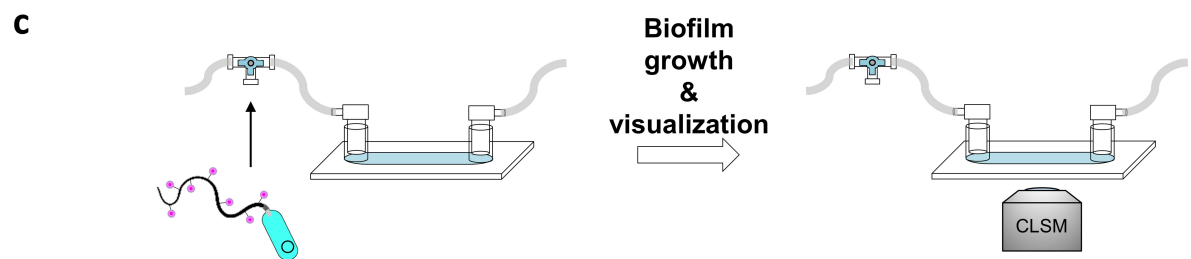
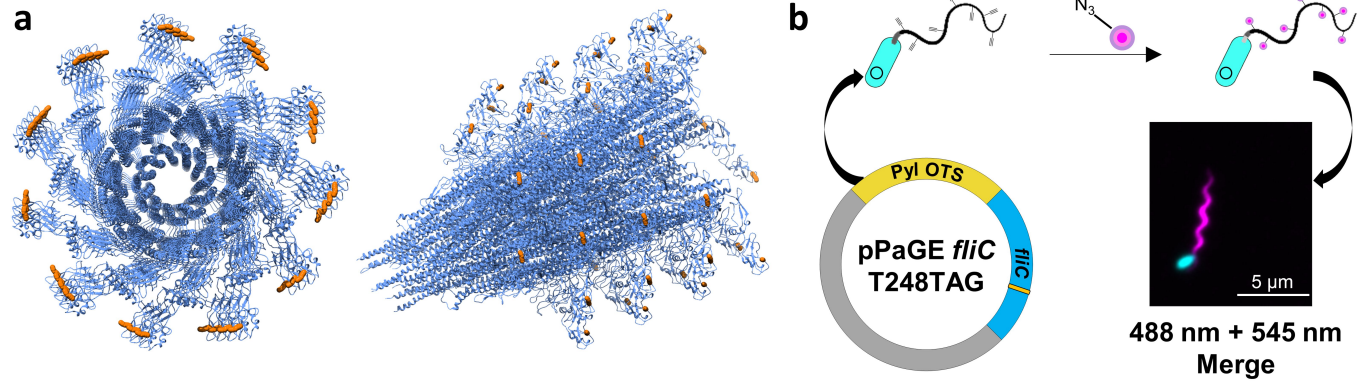
818            57 (2019).

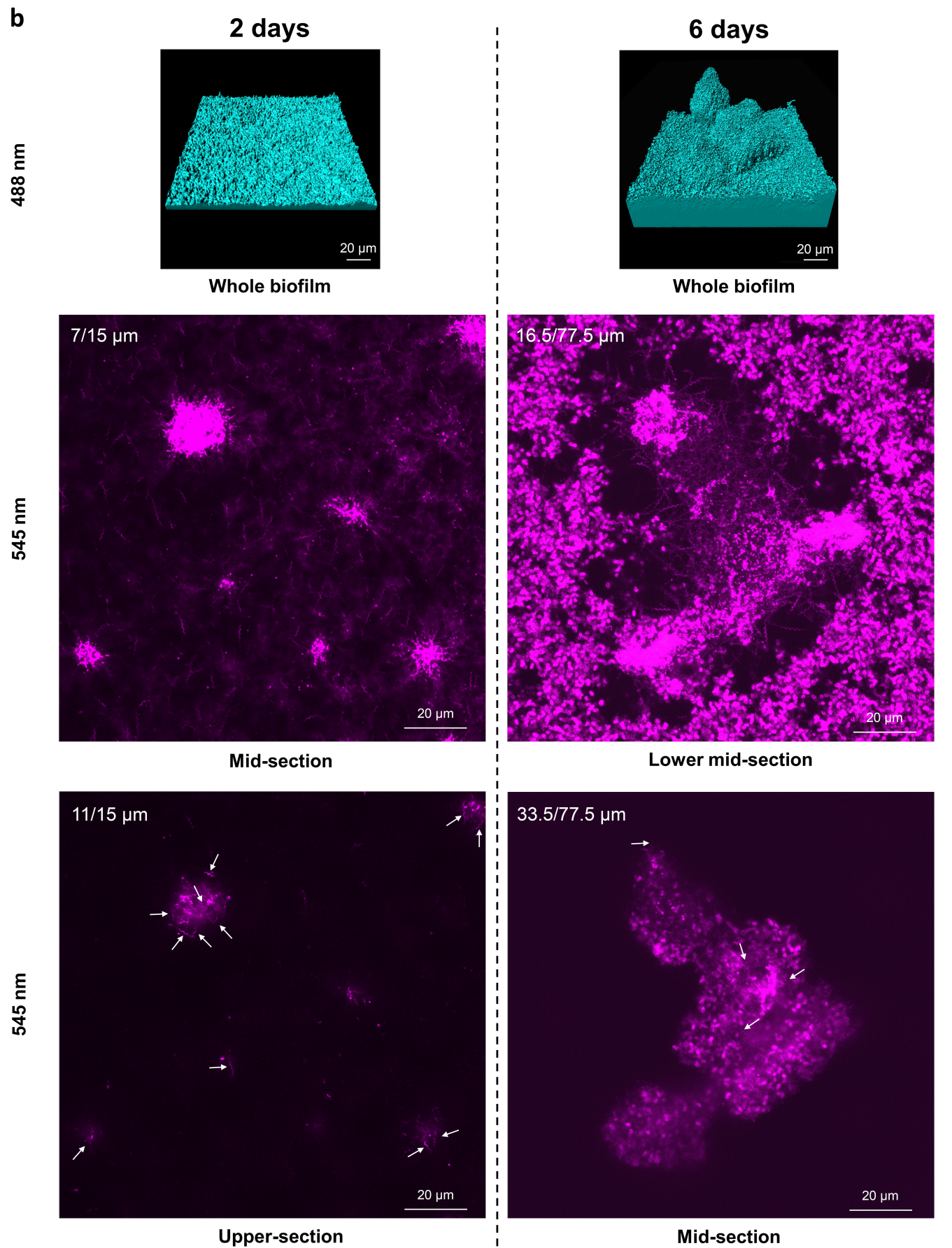
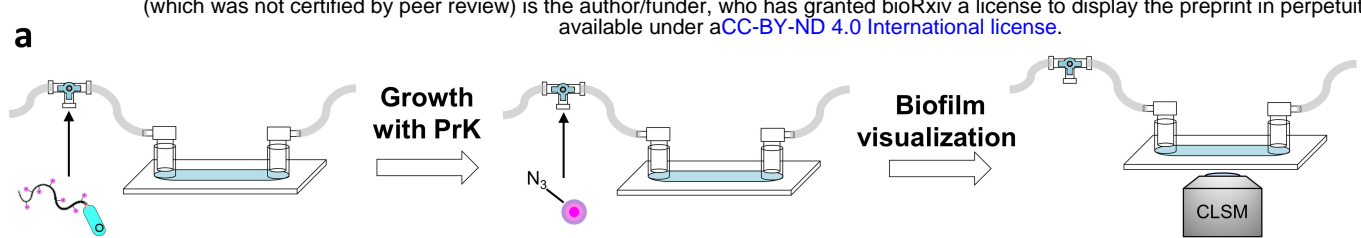
819    57.    Freedman, D. & Diaconis, P. On the histogram as a density estimator:L2 theory.

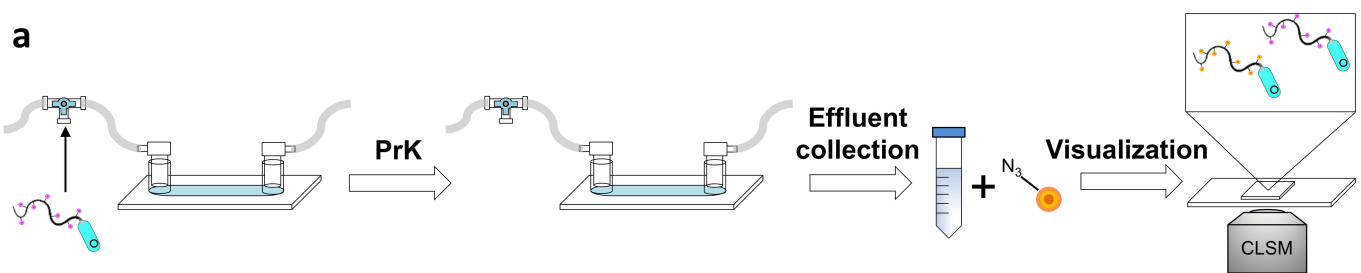
820            *Zeitschrift für Wahrscheinlichkeitstheorie und Verwandte Gebiete* **57**, 453–476 (1981).

821

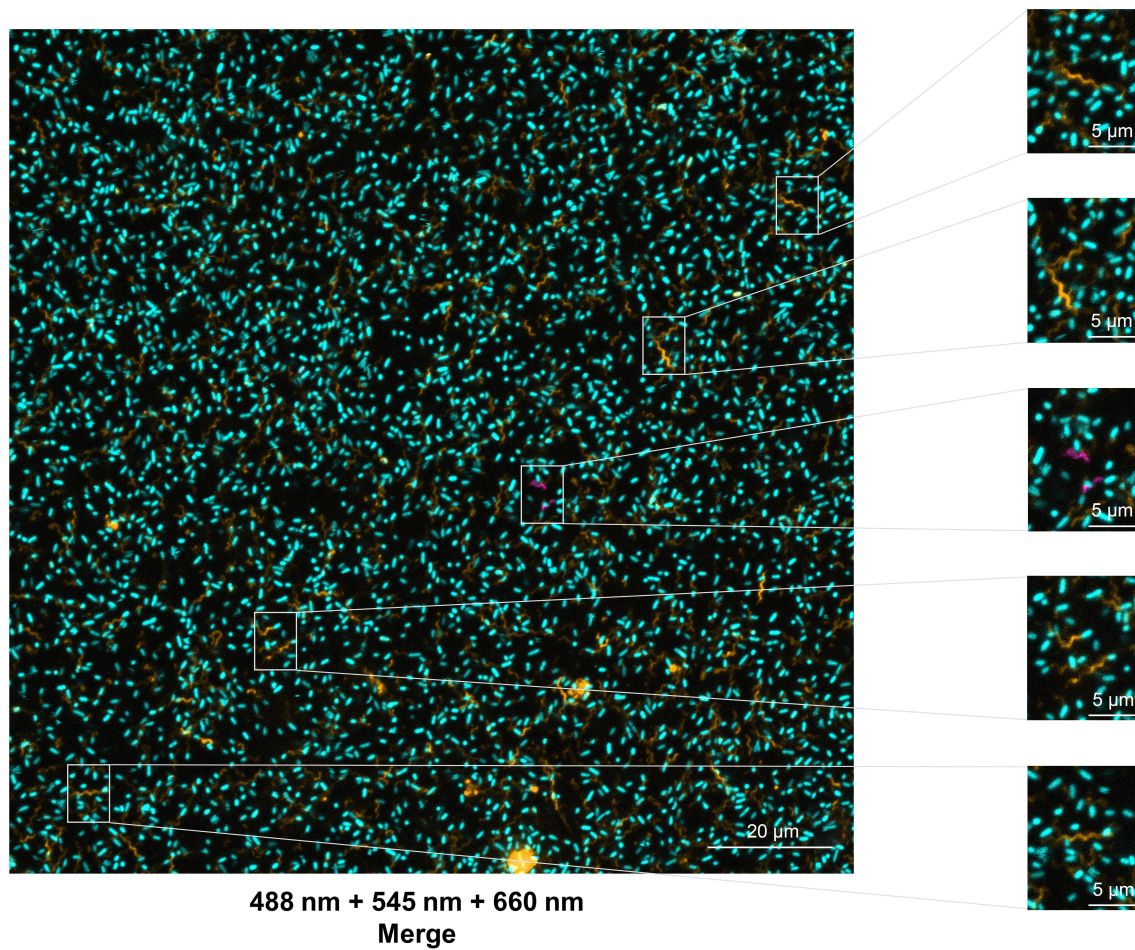










**b**



 - Inoculated bacteria (cyan+black)

 - Divided during biofilm growth (cyan+magenta)

